BEAM GENERATED INSTABILITIES IN SPACE PLASMA

A DISSERTATION

SUBMITTED TO THE DEPARTMENT OF PHYSICS,

UNIVERSITY OF DURBAN-WESTVILLE

IN PARTIAL FULFILLMENT OF THE REQUIREMENTS

FOR THE DEGREE OF

MASTER OF SCIENCE

By

Surversperi Suryakumari Misthry

May 1999

Preface

The work described in this thesis was carried out by the author in the Department of Physics, University of Durban-Westville, from January 1997 to January 1999, under the supervision of Professor R. Bharuthram .

These studies represent original work by the author and have not been submitted in any form to another university. Where use is made of the work of others, it has been duly acknowledged in the text.

TO NARISHA AND MANASH

Acknowledgements

The completion of this thesis would not have been possible without the assistance of the following people.

My supervisor, Professor R. Bharuthram, whose expert guidance of the work in this thesis I sincerely appreciate.

My dear friends Shobana, Sadha and Shimul whose encouragement and assistance I am deeply grateful for.

Dhunsunker for his constant support.

My family Ashwin, Narisha, Manash, Tilly, Mogie and my mother for their support and understanding.

Abstract

Electrostatic instabilities associated with a model applicable to the auroral acceleration region consisting of an ion beam, precipitating electrons and stationary background electrons are theoretically investigated. The kinetic dispersion relation is solved numerically without approximations. It is shown that two low-frequency plasma instabilities are present and these may generate the low-frequency electric field fluctuations (LEFs) that have been observed in the acceleration region.

A parameter variation study is carried out in order to reveal the features of the instabilities. The model is adapted to suit two possible regions of study: (1) drifting cool ions and (2) drifting cool ions and counter-streaming hot electrons.

The slow ion-acoustic instability which dominates at low ion beam drift velocities is studied by varying plasma parameters such as the propagation angle, k_y/k, the wavenumber, k, the cold background electron density, n_{co}, the hot electron temperature and the cool ion beam temperature.

The second mode, the modified two-stream instability, which dominates at larger ion beam drift velocities and at oblique angles of propagation is investigated in a similar manner.

To complete the study of these two instabilities, the effect of drifting hot electrons is

examined briefly through a similar parameter variation study.

List of commonly used symbols

a	n_{oc}/n_o
b	$(n_{oh}/n_o)(T_c/T_h)$
$\mathbf{B_o}$	external magnetic field in the z-direction
c	T_c/T_b
C_b	$(T_b/m_i)^{\frac{1}{2}}$, thermal velocity of ions
C_c	$(T_c/m_e)^{\frac{1}{2}}$, thermal velocity of cold electrons
C_h	$(T_h/m_e)^{\frac{1}{2}}$, thermal velocity of hot electrons
C_s	$(T_e/m_i)^{\frac{1}{2}}$, ion sound speed
e	electronic charge
$\mathbf{E}$	electric field
f_j	distribution function of species j
f_{jo}	equilibrium distribution function of species j
i	$\sqrt{-1}$
I_p	modified Bessel function of order p
J_p	Bessel function of order p
$\mathbf{k}$	wave propagation vector $= (k_x, k_y, k_z)$
$k_\perp$	component of $\mathbf{k}$ perpendicular to $\mathbf{B_o} = B_o\hat{z} = (k_x^2 + k_y^2)^{\frac{1}{2}}$
m_j	mass of species j

n_o	plasma density
n_j	density of species j
n_{jo}	equilibrium density of species j
T_j	temperature of species j
$\mathbf{v}$	velocity vector $= (v_x, v_y, v_z)$
$\mathbf{V_o}$	drift velocity
$v_\perp$	component of $\mathbf{v}$ in the x-y plane $= (v_x^2 + v_y^2)^{\frac{1}{2}}$
v_{dj}	drift velocity of species j
v_{djz}	drift velocity of species j in the z-direction
$\hat{x}, \hat{y}, \hat{z}$	unit vectors in the x, y, z - directions
$Z(\lambda)$	plasma dispersion function with argument λ
α_b	$k_\perp^2 C_b^2/\Omega_i^2$
α_c	$k_\perp^2 C_c^2/\Omega_e^2$
α_h	$k_\perp^2 C_h^2/\Omega_e^2$
Γ_{pj}	$e^{-\alpha_j} I_p(\alpha_j), j = b, c, h$ for the respective species of particles
γ	imaginary part of complex frequency, ω
λ_{dj}	$(T_j/4\pi n_{jo} e^2)$, Debye length of species j
θ	angle between wave vector k and beam velocity
Ψ	angle between k_x and $k_\perp$
ϕ	electrostatic potential
ω	complex frequency
$\bar{\omega}$	$\omega - \mathrm{k}.\mathbf{V_o}$, Doppler shifted frequency
ω_r	real part of ω
ω_{pj}	$(4\pi n_{oj} e^2/m_j)^{\frac{1}{2}}$, plasma frequency of species j
Ω_j	$(eB_o/m_j c)$, gyrofrequency of species j

Contents

List of Figures

Chapter 1

Introduction

The study of plasma instabilities has received much attention in fusion, space and astrophysics research, as well as in industrial plasma applications. Instabilities are classified broadly into macroscopic and microscopic instabilities. Through macroscopic instabilities, the plasma loses its free energy by a distortion of shape. These are usually studied with fluid equations. Microscopic instabilities involve velocity distribution functions of the particles and are studied with the kinetic Boltzmann-Vlasov equations. The plasma loses its free energy through electrostatic or electromagnetic waves. The process by which the free energy of the plasma gets converted into a growing mode in a collective way is called a plasma instability (Lakhina, 1994).

Plasma instabilities have been found to play an important role in many phenomena occuring in astrophysical, space and laboratory plasmas. Many of these plasmas are not in thermodynamic equilibrium and lose their free energy through the excitation of a growing (in amplitude) plasma wave.

Various kinds of microscopic plasma instabilities have been encountered in space environments. S3 – 3, Viking and ROSE satellite observations have provided data

on phenomena such as elevated ion conics, ion acoustic double layers, electrostatic shocks and low-frequency electric field fluctuations (LEFs) on the auroral field lines (Temerin, 1978; Hultqvist et al., 1988; Rose et.al., 1992). The presence of ion beams and accelerating electrons have been the source of several investigations into beam generated electrostatic instabilities in the auroral plasma. Research into instabilities reveal possible mechanisms for the generation of various phenomena that have been observed. In this thesis we examine the instabilities that arise in the auroral plasma located between one and two earth radii (ie. 6000 – 12000 km.). In particular, we study instabilities associated with the generation of LEFs.

Lakhina(1993) discusses the instability associated with a model, applicable to the auroral plasma, consisting of precipitating electrons, a single species H^+ or O^+ ion beam and cold background electrons. In his paper the kinetic dispersion relation is solved analytically, with appropriate approximations in the electrostatic limit, by treating the ion beam as cool and the precipitating electrons as hot.

In this thesis, we adopt the model of Lakhina(1993) and examine the associated instabilities. However, in our case the dispersion relation is completely solved numerically without any approximations and a detailed parameter study is presented. Further, since ion beams parallel to the magnetic field have been found to have thermal energies that are much larger than the ambient thermal energy of their ionospheric source region, (Bergmann and Lotko, 1986), we examine also the effect of increasing the ion beam temperature as well.

The thesis is presented as follows:

In Chapter 2 we review the relevant literature. The Kinetic Dispersion Relation is derived for our model in Chapter 3. Our numerical results are presented in

Chapter 4 (for an ion beam) and Chapter 5 (for counter-streaming electron and ion beams). Finally, Chapter 6 contains a summary of our results and the major conclusions.

Chapter 2

Literature survey

The consistent observations of low frequency turbulence by $S3-3$, Viking and ROSE satellites at altitudes between $6000-12000$km. in the auroral plasma have been the subject of study for many years (Mozer et.al., 1977; Temerin, 1978; Hultqvist et.al., 1988; Rose et.al.,1992; and others). It has been emphasized that LEFs are closely associated with the excitation of various auroral phenomena.

Mozer et.al.(1977) have shown that electrostatic shocks with fields of up to 600 mV/m are embedded in regions of low-frequency and large amplitude electrostatic turbulence on the auroral field lines at altitudes between 1000km and 8000km. From data collected by the $S3-3$ satellite, Temerin(1978) showed that a particular signature of the electric field frequency-time spectrogram, the "resonance fingerprint", indicated that the frequency range of the electrostatic turbulence is dominated by the Doppler shift of zero frequency turbulence.

Further investigations indicated that auroral plasma instabilities could give rise to an oscillating electric field, (Bhatia and Lakhina, 1980). In their paper, the precipitating electrons are regarded as anti-loss-cone electrons which are characterized

by particle distributions having a deficit of particles with $v_{||} \approx 0$. i.e. they have a large velocity spread parallel to the magnetic field lines. The streaming motion of these energetic electrons is shown to produce a low-frequency electrostatic instability (n= 0, Bernstein mode) which can give rise to an oscillating electric field, E$\approx 0.5-25$ mV/m.

Bergmann and Lotko (1986) investigated two instabilities viz. the H^+-O^+ two stream instability and a resonant electron-ion instability. The following observed features of the auroral plasma were found to be important:

1. the various plasma parameters vary with the electric field potential (and consequently altitude) along the geomagnetic field lines.

2. the dominant plasma species at the low-altitude end are cool compared to those at the magnetospheric end.

3. the effective ratio of T_e/T_i initially increases with altitude.

4. the upward accelerated ions are adiabatically cooled.

It was also found that low altitude plasmas were dominated by 2 species of ions and warm electrons, while in the magnetospheric region, only H^+ existed together with thermal electrons.

The H^+-O^+ two-stream instability was further examined in a magnetised and an unmagnetised plasma for application to ion beam heating in the auroral electron acceleration region. (Bergmann et.al., 1988). Wave modes which propagated obliquely to the magnetic field were investigated. These investigations showed that heating of the ion beams does develop at an oblique angle to the magnetic field. Dusenbery

et.al.(1988) also studied the excitation of low-frequency electrostatic modes by the ion-ion two-stream instability for auroral plasma parameters.

Many interesting phenomena were associated with the presence of LEFs by several authors. The analysis of data from Viking observations in 1986 by Hultqvist et.al. (1988) confirmed the existence of accelerating electrons and ions along magnetic field lines by quasi-static electric fields. Further studies on these satellite observations by Hultqvist(1988) revealed that the simultaneous observation of upward field-aligned fluxes of energetic ions and electrons may be due to field-aligned electric fields. It was pointed out in this paper that for the electrons, the fluctuating electric field appears as quasi-static. This results in electrons leaving the acceleration region in an effective half-period of the field when it points downward. The fluctuating field has only a small effect on the ions which are accelerated upward only by the magnetic-field-aligned dc component of the electric field.

A close correlation between the presence of LEFs and of upstreaming electrons, as well as elevated ion conics, on the auroral field lines was found by Ashour-Abdalla and Schriver (1989). In this study, through a self-consistent particle simulation, the presence of a steady state electric field was assumed and seen to generate a low-frequency ion-ion two-stream instability. This instability in turn created a fluctuating field that heated the ions oblique to the magnetic field forming distributions similar to ion conics.

Lakhina(1993), brought the focus back to the cause of LEFs themselves. Previous studies mentioned earlier discussed the generation of LEFs by the ion-ion two stream instability where the free energy for the instability is derived from the relative streaming of the ion species. In this paper, precipitating electrons and upward

moving ion beams in the presence of cold background electrons were shown to drive a low- frequency electrostatic instability. Two modes of the ion beam instability were discussed, (one at high drift velocities and the other at low drift velocities), and a resonant instability driven by hot electrons. The low frequency modes were found to have a broadband spectrum and were easily excited either by ion beams having drift speeds in the range $100 - 1500$ km.s^{-1}, or by precipitating electrons drifting with speed ≥ 5000 km.s^{-1} along the field lines. The results were found to be in fairly good agreement with observations from Viking (Hultqvist et.al., 1988) and S3−3 (Temerin, 1978). Heating of ions and electrons was found possible only in the direction parallel to the magnetic field. This led to the formation of hot electron and ion beams. The presence of the cold background component in the model was found to be essential for the formation of these modes.

Data on the electric field fluctuations detected by probes on the ROSE F4 rocket was recently analysed by Iranpour et.al.(1997). The results showed that the waves propagate in the Hall-current direction with a velocity below the ion-sound speed. It was also found that the waves are dispersive.

Chapter 3

Derivation of the Kinetic Dispersion Relation

To derive the kinetic dispersion relation for low-frequency electrostatic waves, we follow the method of Gary and Sanderson(1970) and Singh and Bharuthram(1990). The plasma in the auroral acceleration region is described by a model consisting of three species in a homogeneous, collisionless plasma embedded in a uniform geomagnetic field, $\mathbf{B_0}$, which is taken to be in the z-direction. These particles are: precipitating hot electrons streaming down the geomagnetic field lines with drift velocity $\mathbf{v_{dh}} = -v_{dhz}\hat{z}$, temperature T_h and density n_h; cold stationary background electrons with temperature T_c and density n_c and an ion beam (H^+) moving upward away from the earth along the auroral field lines with drift velocity $\mathbf{v_{db}} = v_{dbz}\hat{z}$, temperature T_b and density n_b. The distribution functions for the hot electrons and the ions are considered as drifting Maxwellians while the cold background electrons have a stationary Maxwellian distribution function. For charge neutrality at equilibrium we require

$$n_{b0} = n_{c0} + n_{h0}$$

where n_{j0} is the equilibrium density of the species j.

3.1 The Ion Beam Term

We consider the ion beam velocity distribution as an isotropic, drifting Maxwellian with temperature T_b, drifting parallel to the magnetic field, $\mathbf{B_0} = B_0\hat{z}$, with drift velocity $\mathbf{v_{dbz}}$. This is depicted in figure (3.1).

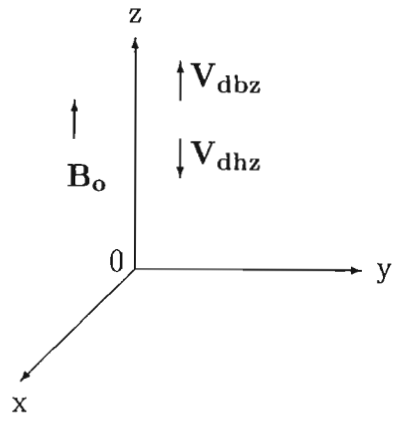

Figure (3.1)

The equilibrium velocity distribution for the ion beam is then given by

$$f_{b0} = \frac{n_{b0}}{(2\pi C_b^2)^{\frac{3}{2}}} \exp\left[-\frac{v_x^2 + v_y^2 + (v_z - v_{dbz})^2}{2C_b^2}\right], \tag{3.1}$$

where $C_b = (T_b/m_i)^{\frac{1}{2}}$ is the thermal velocity of the ions.

Neglecting collisions and considering only the effects of electromagnetic forces, we may use the Vlasov equation

$$\frac{\partial f_b}{\partial t} + \mathbf{v}.\nabla f_b + \frac{e}{m}(\mathbf{E} + \mathbf{v} \times \mathbf{B}).\frac{\partial f_b}{\partial \mathbf{v}} = 0. \tag{3.2}$$

By considering small **electrostatic** perturbations about the equilibrium quantities,

$$\left.\begin{aligned} f_b &= f_{b0}(\mathbf{v}) + f_{b1}(\mathbf{v}) \\ \mathbf{E} &= \mathbf{E_0} + \mathbf{E_1} \end{aligned}\right\} \tag{3.3}$$

we linearize the Vlasov equation. Substituting (3.3) into (3.2) and linearizing, we obtain:

$$\partial_t f_{b_1} + \mathbf{v}.\nabla f_{b_1} + \frac{e}{m_i}\mathbf{E_1}.\partial_{\mathbf{v}} f_{b0} + \frac{e}{m_i}(\mathbf{E_0} + \frac{\mathbf{v} \times \mathbf{B_0}}{c}).\partial_{\mathbf{v}} f_{b1} = 0. \tag{3.4}$$

In the absence of an equilibrium electric field we have $\mathbf{E_0} = 0$ and we note that for electrostatic fluctuations: $\mathbf{E_1} = -\nabla\phi_1$ since $\mathbf{B_1} = 0$. With $\mathbf{B_0} = B_0\hat{z}$, (3.4) reduces to

$$\frac{df_{b_1}}{dt} + \frac{e}{m_i}(-\nabla\phi_1).\partial_{\mathbf{v}} f_{b0} = 0 \quad ,$$

which implies that

$$\frac{df_{b1}}{dt} = \frac{e}{m_i}\nabla\phi_1.\partial_{\mathbf{v}} f_{b0}$$

where the operator $d/dt = (\partial_t + \mathbf{v}.\nabla)$ is defined as the rate of change following an unperturbed orbit in phase space. Integrating along the unperturbed orbits we obtain:

$$f_{b1}(\mathbf{r}, \mathbf{v}, t) = \frac{e}{m_i}\int_{-\infty}^{t} \nabla\phi_1(r', t').\partial_{\mathbf{v}'} f_{b0}(\mathbf{v}')dt' \quad , \tag{3.5}$$

where

$$\mathbf{v}' = \frac{d\mathbf{r}'}{dt'}, \qquad \frac{d\mathbf{v}'}{dt'} = \frac{e}{m_i}\left[\mathbf{E_0} + \frac{\mathbf{v}' \times \mathbf{B_0}}{c}\right],$$

and

$$\mathbf{r}'(0) = \mathbf{r},$$
$$\mathbf{v}'(0) = \mathbf{v}.$$

We have assumed above that the plasma is undisturbed at $t = -\infty$. Differentiating (3.1) we get:

$$\begin{aligned}\partial_{\mathbf{v}'} f_{b0} &= \frac{n_{b0}}{(2\pi C_b^2)^{\frac{3}{2}}} \exp\left[-\frac{(v_x')^2 + (v_y')^2 + (v_z' - v_{dbz})^2}{2C_b^2}\right] \\ &\quad \times \left[-\left(\frac{v_x'\hat{x} + v_y'\hat{y} + (v_z' - v_{dbz})\hat{z}}{C_b^2}\right)\right] \\ &= -\left(\frac{v_x'}{C_b^2}, \frac{v_y'}{C_b^2}, \frac{v_z' - v_{dbz}}{C_b^2}\right) f_{b0}(\mathbf{v}'), \end{aligned} \tag{3.6}$$

or we may write

$$\partial_{\mathbf{v}'} f_{b0} = -\mathbf{v_{eq}} f_{b0}(\mathbf{v}'), \tag{3.7}$$

where

$$\mathbf{v_{eq}} = \left(\frac{v_x'}{C_b^2}, \frac{v_y'}{C_b^2}, \frac{v_z' - v_{dbz}}{C_b^2}\right).$$

For perturbations that are harmonic in space and time, we may write

$$\left.\begin{aligned} f_{b1}(\mathbf{r}, \mathbf{v}, t) &= f_{b1}(\mathbf{v}) \exp\{i(\mathbf{k}.\mathbf{r} - \omega t)\} \\ \phi_1(\mathbf{r}, t) &= \phi_{k\omega} \exp\{i(\mathbf{k}.\mathbf{r} - \omega t)\} \end{aligned}\right\}. \tag{3.8}$$

Substituting into (3.5) we get:

$$f_{b1}(\mathbf{r},\mathbf{v},t) = -\frac{ie}{m_i} f_{b0}(\mathbf{v}') \int_{-\infty}^{t} \mathbf{k}.\mathbf{v_{eq}} \phi(\mathbf{r}',t')dt'. \tag{3.9}$$

Solving the ion equation of motion

$$m\frac{d\mathbf{v}}{dt} = q\left\{\mathbf{E} + \frac{\mathbf{v}\times\mathbf{B}}{c}\right\}$$

we obtain

$$\left.\begin{aligned} v'_x &= v'_\perp \cos(-\Omega_i t' + \theta) \\ v'_y &= v'_\perp \sin(-\Omega_i t' + \theta) \\ v'_z &= constant \end{aligned}\right\} \tag{3.10}$$

where

$$v'_\perp = \left\{(v'_x)^2 + (v'_y)^2\right\}^{\frac{1}{2}},$$

is the velocity perpendicular to the magnetic field lines and $\Omega_i = eB_0/m_i c$ is the ion gyrofrequency.

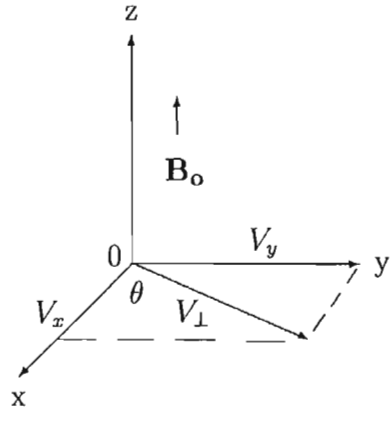

Figure (3.2)

The situation at $t' = 0$ is illustrated in figure (3.2), with $\mathbf{v}'(0) = \mathbf{v} = [v_\perp \cos\theta, v_\perp \sin\theta, v_z]$.

In order to allow for the different gyration directions of the ions and electrons, the coefficient of Ω_i is made negative for the ions which have angular momentum vectors antiparallel to $\mathbf{B_0}$. Since motion along the field lines is unaffected by the field, v'_z =constant. The wave vector $\mathbf{k}$ may be resolved into components parallel and perpendicular to $\mathbf{B_0}$ as shown in figure (3.3).

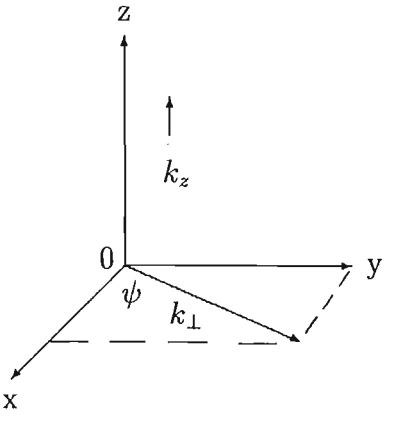

Figure (3.3.)

Hence we have

$$\mathbf{k} = [k_x, k_y, k_z) = (k_\perp \cos\Psi, k_\perp \sin\Psi, k_z]\,, \tag{3.11}$$

and we may write

$$\begin{aligned} \mathbf{k}.\mathbf{v_{eq}} &= [k_x, k_y, k_z] \cdot \left[\frac{v'_x}{C_b^2}, \frac{v'_y}{C_b^2}, \frac{v'_z - v_{dbz}}{C_b^2}\right] \\ &= \frac{k_\perp v'_\perp}{C_b^2}\cos(\Omega_i t' + \Psi - \theta) + \frac{k_z(v'_z - v_{dbz})}{C_b^2}\,. \end{aligned} \tag{3.12}$$

Using (3.8) and (3.11), we may write (3.9) as follows:

$$
\begin{aligned}
& f_{b1}(\mathbf{r},\mathbf{v},t) \\
= \; & f_{b1}(\mathbf{v})\exp\{i(\mathbf{k}.\mathbf{r}-\omega t)\} \\
= \; & -\frac{ie}{m_i}f_{b0}(\mathbf{v}')\int_{-\infty}^{t}\left\{\frac{k_\perp v'_\perp}{C_b^2}\cos(\Omega_i t'+\Psi-\theta)+\frac{k_z(v'_z-v_{dbz})}{C_b^2}\right\}\phi_1(\mathbf{r}',t')dt' \\
= \; & -\frac{ie}{m_i}f_{b0}(\mathbf{v}')\left\{\frac{k_\perp v'_\perp}{C_b^2}\int_{-\infty}^{t}\phi_1\cos(\Omega_i t'+\Psi-\theta)dt'+\frac{k_z(v'_z-v_{dbz})}{C_b^2}\int_{-\infty}^{t}\phi_1 dt'\right\}
\end{aligned}
\tag{3.13}
$$

Evaluating (3.13) at $t=0$, we have:

$$
\begin{aligned}
f_{b1}(\mathbf{v}) = -\frac{ie}{m_i}f_{b0}(\mathbf{v})\phi_{1k\omega}\Bigg[&\frac{k_\perp v_\perp}{C_b^2}\int_{-\infty}^{0}\cos(\Omega_i t'+\Psi-\theta)\times\exp\{i(\mathbf{k}.(\mathbf{r}'-\mathbf{r})-\omega t')\}\,dt' \\
&+\frac{k_z(v_z-v_{dbz})}{C_b^2}\int_{-\infty}^{0}\exp\{i(\mathbf{k}.(\mathbf{r}'-\mathbf{r})-\omega t')\}\,dt'\Bigg]
\end{aligned}
\tag{3.14}
$$

Upon integrating (3.10) we obtain

$$
\mathbf{r}' = \left[-\frac{v'_\perp}{\Omega_i}\sin(-\Omega_i t'+\theta),\frac{v'_\perp}{\Omega_i}\cos(-\Omega_i t'+\theta),v'_z t'\right]. \tag{3.15}
$$

At $t'=0$,

$$
\mathbf{r}'(0)=\mathbf{r}=\left[-\frac{v'_\perp}{\Omega_i}\sin\theta,\frac{v'_\perp}{\Omega_i}\cos\theta,0\right], \tag{3.16}
$$

and from (3.15) and (3.16), with $\mathbf{r}'(0)=\mathbf{r}=[x_0,y_0,z_0]$, we obtain the orbit equations

$$
\begin{aligned}
\mathbf{r}'-\mathbf{r} = \; & \frac{v'_\perp}{\Omega_i}\left[-\sin(\theta-\Omega_i t')+\sin\theta\right]\hat{x} \\
& +\left[\frac{v'_\perp}{\Omega_i}\left\{\cos(\theta-\Omega_i t')-\cos\theta\right\}\right]\hat{y}+\left[v'_z t'\right]\hat{z}.
\end{aligned}
\tag{3.17}
$$

Using (3.11) and (3.17), the second integral in (3.14) becomes

$$\int_{-\infty}^{0} \exp\left[i\mu \sin(\theta - \Psi)\right] \times \exp\left[-i\mu \sin(\theta - \Psi - \Omega_i t')\right] \times \exp\left[i(\mathbf{k}.\mathbf{v_{db}} + k_z(v_z' - v_{dbz}) - \omega\right] t' dt' \tag{3.18}$$

where $\mu = \frac{k_\perp v_\perp'}{\Omega_i}$. With the use of the identity (Watson 1944):

$$\exp(i\mu \sin\beta) = \Sigma_{p=-\infty}^{\infty} \exp(ip\beta) J_p(\mu)\,, \tag{3.19}$$

where J_p is the ordinary Bessel function of the first kind of order p, (3.18) becomes:

$$\int_{-\infty}^{0} \Sigma_{p=-\infty}^{\infty} \exp\left[ip(\theta - \Psi)\right] J_p(\mu) \times \Sigma_{q=-\infty}^{\infty} \exp\left[-iq(\theta - \Psi - \Omega_i t')\right] J_q(\mu) \times \exp\left[i(\mathbf{k}.\mathbf{v_{db}} + k_z(v_z' - v_{dbz}) - \omega)\right] t' dt'$$

$$= \Sigma_{p=-\infty}^{\infty} \Sigma_{q=-\infty}^{\infty} \left\{ \frac{\exp\left[i(p-q)(\theta - \Psi)\right] J_p(\mu) J_q(\mu)}{i\left[q\Omega_i + \mathbf{k}.\mathbf{v_{db}} + k_z(v_z - v_{dbz}) - \omega\right]} \right\} . \tag{3.20}$$

Using the identity

$$\cos\beta = \frac{e^{i\beta} + e^{-i\beta}}{2} \quad , \tag{3.21}$$

we may write

$$\cos(\Omega_i t' + \Psi - \theta) \exp\left\{i\left[\mathbf{k}.(\mathbf{r}' - \mathbf{r}) - \omega t'\right]\right\} =$$
$$\frac{1}{2} \exp\left\{i(\Omega_i t' + \Psi - \theta)\right\} \exp\left\{i\left[\mathbf{k}.(\mathbf{r}' - \mathbf{r}) - \omega t'\right]\right\} +$$
$$\frac{1}{2} \exp\left\{-i(\Omega_i t' + \Psi - \theta)\right\} \exp\left\{i\left[\mathbf{k}.(\mathbf{r}' - \mathbf{r}) - \omega t'\right]\right\} \tag{3.22}$$

Hence the first integral in (3.14) may be written as:

$$\int_{-\infty}^{0}\left\{\frac{1}{2}\exp\left[i(\Omega_i t'+\Psi-\theta)\right]\exp\left[i\left[\mathbf{k}.(\mathbf{r}'-\mathbf{r})-\omega t'\right]\right]\right\}dt'$$
$$+\int_{-\infty}^{0}\left\{\frac{1}{2}\exp\left[-i(\Omega_i t'+\Psi-\theta)\right]\exp\left[i\left[\mathbf{k}.(\mathbf{r}'-\mathbf{r})-\omega t'\right]\right]\right\}dt' \tag{3.23}$$

The first part of (3.23) is evaluated by using the orbit equations (3.17) and the identity (3.19) to yield

$$\frac{1}{2}\Sigma_{p=-\infty}^{\infty}\Sigma_{q=-\infty}^{\infty}\frac{\exp\left[i(p-q-1)(\theta-\Psi)\right]J_p(\mu)J_q(\mu)}{i\left[(q+1)\Omega_i+\mathbf{k}.\mathbf{v_{db}}+k_z(v_z-v_{dbz})-\omega\right]}. \tag{3.24}$$

Similarly the second part yields

$$\frac{1}{2}\Sigma_{p=-\infty}^{\infty}\Sigma_{q=-\infty}^{\infty}\frac{\exp\left[i(p-q+1)(\theta-\Psi)\right]J_p(\mu)J_q(\mu)}{i\left[(q-1)\Omega_i+\mathbf{k}.\mathbf{v_{db}}+k_z(v_z-v_{dbz})-\omega\right]}. \tag{3.25}$$

Using (3.20), (3.24) and (3.25) in (3.14) we obtain the perturbed velocity distribution function:

$$f_{b1}(\mathbf{v})=-\frac{e}{m_i}f_{b0}(\mathbf{v})\phi_{1k\omega}\left[\frac{k_\perp v_\perp}{2C_b^2}\Sigma_{p=-\infty}^{\infty}\Sigma_{q=-\infty}^{\infty}J_p(\mu)J_q(\mu)\times\right.$$

$$\left(\frac{\exp\left\{i(p-q-1)(\theta-\Psi)\right\}}{(q+1)\Omega_i+\mathbf{k}.\mathbf{v_{db}}+k_z(v_z-v_{dbz})-\omega}+\frac{\exp\left\{i(p-q+1)(\theta-\Psi)\right\}}{(q-1)\Omega_i+\mathbf{k}.\mathbf{v_{db}}+k_z(v_z-v_{dbz})-\omega}\right)$$

$$\left.+k_z\frac{(v_z-v_{dbz})}{C_b^2}\Sigma_{p=-\infty}^{\infty}\Sigma_{q=-\infty}^{\infty}\frac{\exp\left\{i(p-q)(\theta-\Psi)\right\}J_p(\mu)J_q(\mu)}{q\Omega_i+\mathbf{k}.\mathbf{v_{db}}+k_z(v_z-v_{dbz})-\omega}\right] \tag{3.26}$$

The perturbed ion beam density is given by

$$n_{b1}(\mathbf{r},t)=n_{b1k\omega}\exp\left\{i(\mathbf{k}.\mathbf{r}-\omega t)\right\}=\int f_{b1}(\mathbf{v})d^3\mathbf{v} \tag{3.27}$$

To evaluate the integral in (3.27), we first transform to cylindrical coordinates in velocity space with

$$d^3\mathbf{v} = v_\perp dv_\perp dv_z d\theta.$$

The triple integral in (3.27) can be separated into three parts corresponding to the terms of $f_{b1}(\mathbf{v})$ in (3.26). From the expression (3.1) for the equilibrium velocity distribution $f_{b0}(\mathbf{v})$, the first part yields:

$$-\frac{\pi e\phi_{1k\omega}k_\perp n_{b0}}{T_{b1}(2\pi C_b^2)^{\frac{3}{2}}} \times \Sigma_{p=-\infty}^{\infty} \int_0^\infty \left[\int_{-\infty}^{\infty} \frac{\exp\left\{-\frac{(v_z-v_{dbz})^2}{2C_b^2}\right\}}{p\Omega_i + \mathbf{k}.\mathbf{v_{db}} + k_z(v_z - v_{dbz}) - \omega} dv_z \right] \times \exp\left\{-\frac{v_\perp^2}{2C_b^2}\right\} J_p(\mu) J_{p-1}(\mu) v_\perp^2 dv_\perp \tag{3.28}$$

where we have used $C_b^2 = T_b/m_i$, and the result

$$\int_0^{2\pi} \exp\{i(p-q-1)\theta\}\, d\theta = \begin{cases} 0, & p \neq q+1 \\ 2\pi, & p = q+1. \end{cases}$$

We now introduce the plasma dispersion function (Fried and Conte 1961), also known as the Z- function, defined by

$$Z(\lambda) = \frac{1}{\sqrt{\pi}} \int_{-\infty}^{\infty} \frac{e^{-x^2}}{x-\lambda} dx \quad ,$$

for $Im(\lambda) > 0$, or alternatively as

$$Z(\lambda) = 2ie^{-\lambda^2} \int_{-\infty}^{i\lambda} e^{-t^2} dt. \tag{3.29}$$

The integral over dv_z in (3.28) can be expressed in terms of the Z-function as

$$-\frac{\pi e\phi_{1k\omega}k_\perp n_{b0}}{T_b(2\pi C_b^2)^{\frac{3}{2}}}\frac{\sqrt{\pi}}{k_z}\Sigma_{p=-\infty}^{\infty}\int_0^\infty J_p(\mu)J_{p-1}(\mu)Z\left[\frac{\omega-\mathbf{k}.\mathbf{v_{db}}-p\Omega_i}{\sqrt{2}k_zC_b}\right] \times\exp\left\{-\frac{v_\perp^2}{2C_b^2}\right\}v_\perp^2dv_\perp \quad . \tag{3.30}$$

Similarly the second part of the integral in (3.27) yields

$$-\frac{\pi e\phi_{1k\omega}k_\perp n_{b0}}{T_b(2\pi C_b^2)^{\frac{3}{2}}}\frac{\sqrt{\pi}}{k_z}\Sigma_{p=-\infty}^{\infty}\int_0^\infty J_p(\mu)J_{p+1}(\mu)Z\left[\frac{\omega-\mathbf{k}.\mathbf{v_{db}}-p\Omega_i}{\sqrt{2}k_zC_b}\right] \times\exp\left\{-\frac{v_\perp^2}{2C_b^2}\right\}v_\perp^2dv_\perp \quad . \tag{3.31}$$

The last part of the integral reduces to:

$$-\frac{e\phi_{1k\omega}n_{b0}}{T_bC_b^2}\Sigma_{p=-\infty}^{\infty}\int_0^\infty\left[1+z_{pb}Z(z_{pb})\right]J_p^2(\mu)v_\perp dv_\perp\exp\left\{-\frac{v_\perp^2}{2C_b^2}\right\}, \tag{3.32}$$

where $z_{pb}=\frac{\omega-\mathbf{k}.\mathbf{v_{db}}-p\Omega_i}{\sqrt{2}k_zC_b}$.

Combining the results (3.30 – 3.32), we obtain

$$n_{b1k\omega}=-\frac{e\phi_{1k\omega}n_{b0}}{C_b^2}\left\{\frac{1}{T_b\sqrt{2}k_zC_b}\Sigma_{p=-\infty}^{\infty}\int_0^\infty p\Omega_iJ_p^2(\mu) Z(z_{pb})\exp\left\{-\frac{v_\perp^2}{2C_b^2}\right\}v_\perp dv_\perp + \frac{1}{T_b}\Sigma_{p=-\infty}^{\infty}\int_0^\infty J_p^2(\mu)\left[1+z_{pb}Z(z_{pb})\right]\exp\left\{-\frac{v_\perp^2}{2C_b^2}\right\}v_\perp dv_\perp\right\}, \tag{3.33}$$

where we have used the identity (Watson 1944)

$$J_{p-1}(\mu) + J_{p+1}(\mu) = \frac{2p}{\mu} J_p(\mu)$$

with $\mu = k_\perp v_\perp / \Omega_i$.

The relation (Watson 1944)

$$\int_0^\infty J_p^2(\beta x) \exp(-\mu x^2) x dx = \frac{1}{2\mu} \exp(-\frac{\beta^2}{2\mu}) I_p(\frac{\beta^2}{2\mu}), \tag{3.34}$$

where I_p, is the Modified Bessel function of the first kind of order p, is used to perform the integration over $dv_\perp$. We then obtain

$$n_{b1k\omega} = -\frac{e\phi_{ik\omega} n_{b0}}{T_b} \times \left\{ \frac{1}{\sqrt{2} k_z C_b} \Sigma_{p=-\infty}^{\infty} p\Omega_i Z(z_{pb}) \exp\left\{ -\frac{k_\perp^2 C_b^2}{\Omega_i^2} \right\} I_p \left\{ \frac{k_\perp^2 C_b^2}{\Omega_i^2} \right\} \right.$$
$$\left. + \Sigma_{p=-\infty}^{\infty} [1 + z_{pb} Z(z_{pb})] \exp\left\{ -\frac{k_\perp^2 C_b^2}{\Omega_i^2} \right\} I_p \left\{ \frac{k_\perp^2 C_b^2}{\Omega_i^2} \right\} \right\}. \tag{3.35}$$

Letting $\alpha_b = k_\perp^2 C_b^2 / \Omega_i^2$, $\Gamma_{pb} = e^{-\alpha_b} I_p(\alpha_b)$ and using the identity (Watson 1944) $\Sigma_{p=-\infty}^{\infty} \Gamma_{pb} = 1$, we can write (3.35) as

$$n_{b1k\omega} = -\frac{e\phi_{1k\omega} n_{b0}}{T_b} \left\{ 1 + \frac{\omega - \mathbf{k}.\mathbf{v}_{db}}{\sqrt{2} k_z C_b} \Sigma_{p=-\infty}^{\infty} Z(z_{pb}) \Gamma_{pb} \right\} \tag{3.36}$$

3.2 Contribution of the cold stationary isotropic background electrons to the dispersion relation

The cold background equilibrium electron distribution is assumed to be a stationary isotropic Maxwellian given by:

$$f_{co} = \frac{n_{co}}{(2\pi C_c^2)^{\frac{3}{2}}} \exp\left\{-\frac{v^2}{2C_c^2}\right\} \tag{3.37}$$

where $C_c = (T_c/m_e)^{\frac{1}{2}}$ is the thermal speed. From the charge neutrality requirement, we have at equilibrium :

$$n_{b0} = n_{co} + n_{h0}.$$

Using an analysis similar to that used in section 3.1, we obtain the perturbation for the background electron density n_{co}. This can also be obtained from (3.36) by replacing e by $(-e)$, setting $T_b = T_c$ and the drift velocity to zero, since the background electrons are stationary.

The cold electron density perturbation is then given by:

$$n_{c1k\omega} = \frac{e\phi_{1k\omega} n_{co}}{T_c}\left\{1 + \frac{\omega}{\sqrt{2}k_z C_c}\Sigma_{p=-\infty}^{\infty} Z(z_{pc})\Gamma_{pc}\right\}, \tag{3.38}$$

where $z_{pc} = \frac{\omega - p\Omega_e}{\sqrt{2}k_z C_c}$, $\Gamma_{pc} = \Gamma_{pc}(\alpha_c) = e^{-\alpha_c} I_p(\alpha_c)$ and $\alpha_c = \frac{k_\perp^2 C_c^2}{\Omega_e^2}$, with Ω_e being the electron gyrofrequency.

3.3 Contribution of the hot isotropic precipitating electrons to the dispersion relation

The equilibrium Maxwellian velocity distribution of the hot isotropic electrons is given by:

$$f_{h0} = \frac{n_{h0}}{(2\pi C_h^2)^{\frac{3}{2}}} \exp\left\{-\frac{v_x^2 + v_y^2 + (v_z - v_{dhz})^2}{2C_h^2}\right\}, \tag{3.39}$$

where $C_h = (T_h/m_e)^{\frac{1}{2}}$ is the hot electron thermal speed and v_{dhz} is the drift velocity along the external magnetic field $\mathbf{B_0}$.

Using an analysis similar to that of section 3.1, we obtain the density perturbation of the hot electrons:

$$n_{h1k\omega} = \frac{e\phi_{ik\omega} n_{h0}}{T_h} \times \left\{1 + \frac{\omega - \mathbf{k}.\mathbf{v}_{dh}}{\sqrt{2}k_z C_h} \Sigma_{p=-\infty}^{\infty} Z(z_{ph})\Gamma_{ph}\right\} \tag{3.40}$$

where $z_{ph} = \frac{\omega - \mathbf{k}.\mathbf{v_{dh}} - p\Omega_e}{\sqrt{2}k_z C_h}$, $\Gamma_{ph} = \Gamma_{ph}(\alpha_h) = e^{-\alpha_h} I_p(\alpha_h)$, and $\alpha_h = \frac{k_\perp^2 C_h^2}{\Omega_e^2}$.

3.4 The Kinetic Dispersion Relation

In the electrostatic approximation, Poisson's equation,

$$\nabla^2 \phi = 4\pi e(n_c + n_h - n_b), \tag{3.41}$$

reduces to :

$$-k^2 \phi_{1k\omega} = 4\pi e(n_{c1k\omega} + n_{h1k\omega} - n_{b1k\omega}). \tag{3.42}$$

where the subscript "1" indicates perturbed quantities.

By substituting the density perturbations (3.36),(3.38) and (3.40) into (3.42), we obtain the dispersion relation:

$$-k^2 = \frac{1}{\lambda_{dc}^2}\left\{1 + \frac{\omega}{\sqrt{2}k_z C_c}\Sigma_{p=-\infty}^{\infty} Z(z_{pc})\Gamma_{pc}\right\} + \frac{1}{\lambda_{dh}^2}\left\{1 + \frac{\omega - \mathbf{k}.\mathbf{v}_{dh}}{\sqrt{2}k_z C_h}\Sigma_{p=-\infty}^{\infty} Z(z_{ph})\Gamma_{ph}\right\}$$

$$+\frac{1}{\lambda_{db}^2}\left\{1 + \frac{\omega - \mathbf{k}.\mathbf{v}_{db}}{\sqrt{2}k_z C_b}\Sigma_{p=-\infty}^{\infty} Z(z_{pb})\Gamma_{pb}\right\} \qquad (3.43)$$

where the Debye lengths are $\lambda_{dj} = (T_j/4\pi n_{j0}e^2)^{\frac{1}{2}}, j = c, h, b$ for the cold background electrons, the hot precipitating electrons and the beam ions respectively. Further, since

$$z_{pc} = \frac{\omega - p\Omega_e}{\sqrt{2}k_z C_c},$$

$$z_{ph} = \frac{\omega - \mathbf{k}.\mathbf{v_{dh}} - p\Omega_e}{\sqrt{2}k_z C_h}$$

and

$$z_{pb} = \frac{\omega - \mathbf{k}.\mathbf{v_{db}} - p\Omega_i}{\sqrt{2}k_z C_b},$$

equation (3.43) may then be written in the compact form as:

$$-k^2 = \frac{1}{\lambda_{dc}^2}(1 + z_{0c}\Sigma_{p=-\infty}^{\infty} Z(z_{pc})\Gamma_{pc}) +$$

$$\frac{1}{\lambda_{dh}^2}\left\{1 + z_{0h}\Sigma_{p=-\infty}^{\infty} Z(z_{ph})\Gamma_{ph}\right\} + \frac{1}{\lambda_{db}^2}\left\{1 + z_{0b}\Sigma_{p=-\infty}^{\infty} Z(z_{pb})\Gamma_{pb}.\right\} \qquad (3.44)$$

Substituting $\lambda_{dj} = V_{tj}/\omega_{pj}$ and considering low frequency, electrostatic modes (Bernstein modes, p=0) we may write :

$$1 + X_c + X_h + X_b = 0 \qquad (3.45)$$

where

$$X_j = \frac{\omega_{pj}^2}{k^2 V_{tj}^2} \{1 + z_{oj} Z(z_{oj}) \Gamma_{pj}\} \tag{3.46}$$

which is the dispersion relation obtained by Bhatia and Lakhina(1980) and Bergmann et.al.(1988). Lakhina(1993) discusses approximate solutions to the above dispersion relation.

3.5 Approximate solutions to the dispersion relation

We consider low frequency electrostatic waves driven by a cool ion beam.

For the case of cold background electrons, hot stationary electrons and a cool ion beam, satisfying $T_h \gg T_c, T_b \approx 0$, we have:

$$\mid z_{0c} \mid = \mid \frac{\omega}{\sqrt{2} k_z C_c} \mid \gg 1 \tag{3.47}$$

$$\mid z_{0h} \mid = \mid \frac{\omega}{\sqrt{2} k_z C_h} \mid \ll 1 \tag{3.48}$$

$$\mid z_{0b} \mid = \mid \frac{\omega - \mathbf{k}.\mathbf{v_{db}}}{\sqrt{2} k_z C_b} \mid \gg 1 \tag{3.49}$$

The power series and asymptotic expansions for the Z-function in these limits are given by Fried and Conte (1961):

$$Z(z) = i\sqrt{\pi}\delta \exp(-z^2) - 2z\left[1 - \frac{2z^2}{3} + \frac{4z^4}{15} - ...\right],$$

for $\mid z \mid \ll 1$, and

$$Z(z) = i\sqrt{\pi}\delta \exp(-z^2) - \frac{1}{z}\left[1 + \frac{1}{2z^2} + \frac{3}{4z^4} + ...\right],$$

for $\mid z \mid \gg 1$, where $\delta = \begin{cases} 0, & Im(z) > 0 \\ 1, & Im(z) = 0 \\ 2, & Im(z) < 0 \end{cases}$

For the very low-frequency waves we have $\mid \omega - \mathbf{k}.\mathbf{v_{db}} \mid \ll \Omega_b$. Thus we retain only the $p = 0$ terms in the summations in (3.44).

For an instability (i.e. a growing wave with Im(z) > 0), the first term of (3.44) may now be written as:

$$\frac{1}{\lambda_{dc}^2}\left\{1 + z_{0c}\left[-\frac{1}{z_{0c}}(1 + \frac{1}{2z_{0c}^2})\right]\right\}. \tag{3.50}$$

The approximation for the second term, considering (3.48), becomes:

$$\frac{1}{\lambda_{dh}^2}\left\{1 + z_{0h}(i\sqrt{\pi} - 2z_{0h})\right\}, \tag{3.51}$$

while for the cool ion beam term, we have:

$$\frac{1}{\lambda_{db}^2}\left\{1 + z_{0b}\left[-\frac{1}{z_{0b}}(1 + \frac{1}{2z_{0b}^2})\right]\right\}. \tag{3.52}$$

Combining the terms reduces (3.44) to:

$$-k^2 = \frac{1}{\lambda_{dc}^2}\left\{-\frac{1}{2z_{0c^2}}\right\} + \frac{1}{\lambda_{dh}^2}\left\{1 + i\sqrt{\pi}z_{0h}\right\} + \frac{1}{\lambda_{db}^2}\left\{-\frac{1}{2z_{0b^2}}\right\}. \tag{3.53}$$

Then substituting (3.47) - (3.49) into (3.53) and multiplying by $\lambda_{de}^2 = T_c/4\pi n_o e^2$, we get

$$-k^2\lambda_{de}^2 = a\left\{-\frac{k_z^2 C_c^2}{\omega^2}\right\} + b\left\{1 + \frac{i\sqrt{\pi}\omega}{\sqrt{2}k_z C_h}\right\} + c\left\{-\frac{k_z^2 C_b^2}{\bar{\omega}^2}\right\}, \tag{3.54}$$

where $\bar{\omega} = (\omega - \mathbf{k}.\mathbf{V_o})$, is the Doppler shifted frequency, a $= \lambda_{de}^2/\lambda_{dc}^2 = n_{oc}/n_o$, b $= \lambda_{de}^2/\lambda_{dh}^2 = (n_{oh}/n_o)\ (T_c/T_h)$ and c $= \lambda_{de}^2/\lambda_{db}^2 = T_c/T_b$.

We solve the equation by first writing ω as $\omega = \omega_r + i\gamma$ and assuming that

$$| \gamma/\omega_r | << 1 \text{ and}$$
$$| \gamma/\bar{\omega}_r | << 1 \ .$$

With these assumptions, we make the following approximations :

$$\frac{1}{\omega^2} = \frac{1}{\omega_r^2(1 + 2i\frac{\gamma}{\omega_r})^2} \approx \frac{1}{\omega_r^2}(1 - 2i\frac{\gamma}{\omega_r}),$$

and

$$\frac{1}{\bar{\omega}^2} = \frac{1}{\bar{\omega}_r^2(1 + 2i\frac{\gamma}{\bar{\omega}_r})^2} \approx \frac{1}{\bar{\omega}_r^2}(1 - 2i\frac{\gamma}{\bar{\omega}_r})$$

Using these approximations we have

$$-k^2\lambda_{de}^2 = a\left\{-\frac{k_z^2C_c^2(1 - 2i\frac{\gamma}{\omega_r})}{\omega_r^2}\right\} + b\left\{1 + \frac{i\sqrt{\pi}\omega_r(1 + i\frac{\gamma}{\omega_r})}{\sqrt{2}k_zC_h}\right\} + c\left\{-\frac{k_z^2C_b^2(1 - 2i\frac{\gamma}{\bar{\omega}_r})}{\bar{\omega}_r^2}\right\}. \tag{3.55}$$

Taking the real part of (3.55) we obtain:

$$-k^2\lambda_{de}^2 = a\left\{-\frac{k_z^2C_c^2}{\omega_r^2}\right\} + b + c\left\{-\frac{k_z^2C_b^2}{\bar{\omega}_r^2}\right\}, \tag{3.56}$$

which is fourth order in ω_r. We note that in the absence of the cold electron component ($n_{oc} = 0$, i.e. $a = 0$), (3.56) yields

$$\omega_r = \mathbf{k}.\mathbf{V_o} \pm \frac{k_zC_s}{\sqrt{1 + k^2\lambda_{dh}^2}} \tag{3.57}$$

where $C_s = \sqrt{T_h/m_i}$ is the ion sound speed corresponding to the hot electrons. Equation (3.57) is the usual form of the fast and slow beam ion acoustic waves.

In this limit, (a=0), the imaginary part of (3.55) yields:

$$\frac{\gamma}{\omega_r} = \frac{b\sqrt{\frac{\pi}{8}}\bar{\omega}_r^2(\mathbf{k}.\mathbf{V_o} - \omega_r)}{ck_z^3 C_h C_b^2}. \tag{3.58}$$

For wave growth ($\gamma > 0$), we require $\mathbf{k}.\mathbf{V_o} > \omega_r$. For $\mathbf{V_o} = V_o\hat{z}$, this implies $V_o > \omega_r/k_z$, i.e. the wave phase speed, $v_{\phi_z} = \omega_r/k_z$, along $\mathbf{B_o}$ 'sees' a positive slope of the ion velocity distribution.

Substituting for $\bar{\omega}_r$ from (3.57) we obtain:

$$\frac{\gamma}{\omega_r} = \sqrt{\frac{\pi}{8}}\sqrt{\frac{m_e}{m_i}}\frac{1}{(1+k^2\lambda_{dh}^2)^{\frac{3}{2}}}. \tag{3.59}$$

Chapter 4

Parameter variation study of the ion beam driven ion acoustic and modified two stream instabilities

4.1 Introduction

In this chapter, the dispersion relation (3.45) is solved numerically without any approximations. We consider the case of cool ions drifting along $\mathbf{B_0}$. In the next chapter the effect of a drifting(precipitating) electron component will be considered. A study of the variation of plasma parameters is made in order to determine the characteristics of the instability and thereby identify the modes present. Our results are presented in normalized form.

For the study, an H^+ beam is assumed, with $m_i/m_e = 1836$. Time is normalized by the inverse of the ion plasma frequency, $\omega_{pi} = (4\pi n_0 e^2/m_i)^{\frac{1}{2}}$, spatial lengths by $\lambda_{de} = (T_c/4\pi n_0 e^2)^{\frac{1}{2}}$, speed by the ion sound speed, $C_s = \omega_{pi}\lambda_{de} = (T_c/m_i)^{\frac{1}{2}}$, densities

by the total equlibrium density, n_0, and temperature by the cold electron temperature, T_c.

The normalized standard parameters used for the cool ion beam instability are : ion beam temperature $T_b/T_c = 10$, hot electron temperature $T_h/T_c = 1000$, $n_{co}/n_0 = 0.001$, $\Omega_i/\omega_{pi} = 0.476$, $k\lambda_{de} = 0.01$ for fixed k studies and $v_{dbz} = 100C_s$ for fixed drift speed studies. The choice of these parameters is based on data collected through satellite observations in the auroral acceleration region (Lakhina, 1993). We note that the background electrons are relatively cold.

4.2 Beam driven instabilities

Beam driven instabilities fall into the class of plasma instabilities called microinstabilities (or kinetic instabilities) which depend on the velocity distributions of the plasma species. The energy driving the instability is obtained from the relative drift of the species in the model. We investigate the instability by varying the drift velocity of the ion beam.

It was found that for lower drifts the ion acoustic instability (IAI) dominated while at higher drifts the modified two stream instability (MTSI) dominated. The features of these two instabilities were revealed through a parameter variation study of each.

4.3 The ion-acoustic instability (IAI)

4.3.1 Variation of propagation angle, $_y$

In figure (4.1) the normalized real frequency, ω_r/ω_{pi}, is plotted against $k_y/k = sin\theta$ ($\theta = \theta(\mathbf{k}, \mathbf{B_0})$) for normalized drifts v_{dbz} = 30, 40, 60, 80 and 100, while the corresponding normalized growth rate curves, γ/ω_{pi}, are shown in figure (4.2).

The normalized wave number, k, is set at 0.01. The condition that the electron temperature be sufficiently larger than the ion temperature for electrostatic ion beam instabilities, (Gary and Omidi,1986), is satisfied by our parameters ($T_h/T_c = 100T_b/T_c$).

The instability is seen to propagate with maximum real frequency and growth rate for $\mathbf{k} \parallel \mathbf{v_{dbz}}$. This has been found consistently to be the case for the ion-acoustic mode. An increase in the maximum growth rate is also observed for increasing drift speed thereby indicating a dependence on the beam speed. For $\theta = 0°$, γ/ω_{pi} ranges from 0.072 to 0.704 for normalized drifts ranging from 30 to 100. We find a rapid drop to zero growth rate at higher drifts,while a gradual drop is seen at lower drifts.

Considering the ion-acoustic instability, we have the real frequencies for the fast and slow ion beam modes given by:

$$\omega_r = \mathbf{k}.\mathbf{v_d} \pm \frac{k_z C_s}{(1 + k^2\lambda_{de}^2 + k_\perp^2\rho_s^2)^{\frac{1}{2}}}, \tag{4.1}$$

for a plasma with magnetized electrons and ions (Singh et.al., 1990). For parallel propagation, $k_\perp = 0$. Equation (4.1) then becomes:

$$\omega_r = kv_d \pm \frac{k_z C_s}{(1 + k^2\lambda_{de}^2)^{\frac{1}{2}}}. \tag{4.2}$$

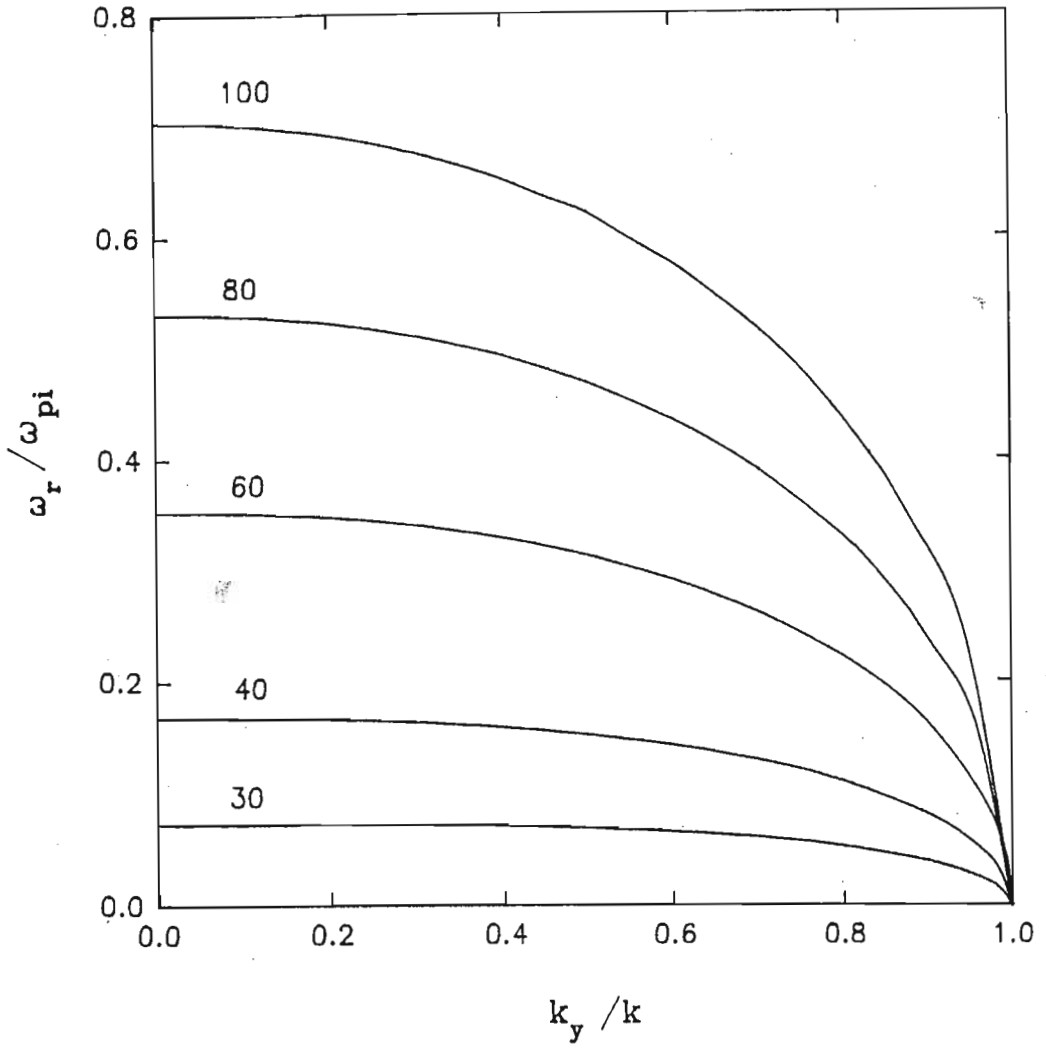

Figure 4.1: Normalized real frequency versus k_y/k with fixed normalized parameters; k=0.01, $T_b/T_c = 10$, $T_h/T_c = 1000$, $n_{co} = 0.001$ and $\Omega_i/\omega_{pi} = 0.476$. The parameter labelling the curves is the ion beam speed, v_{dbz}.

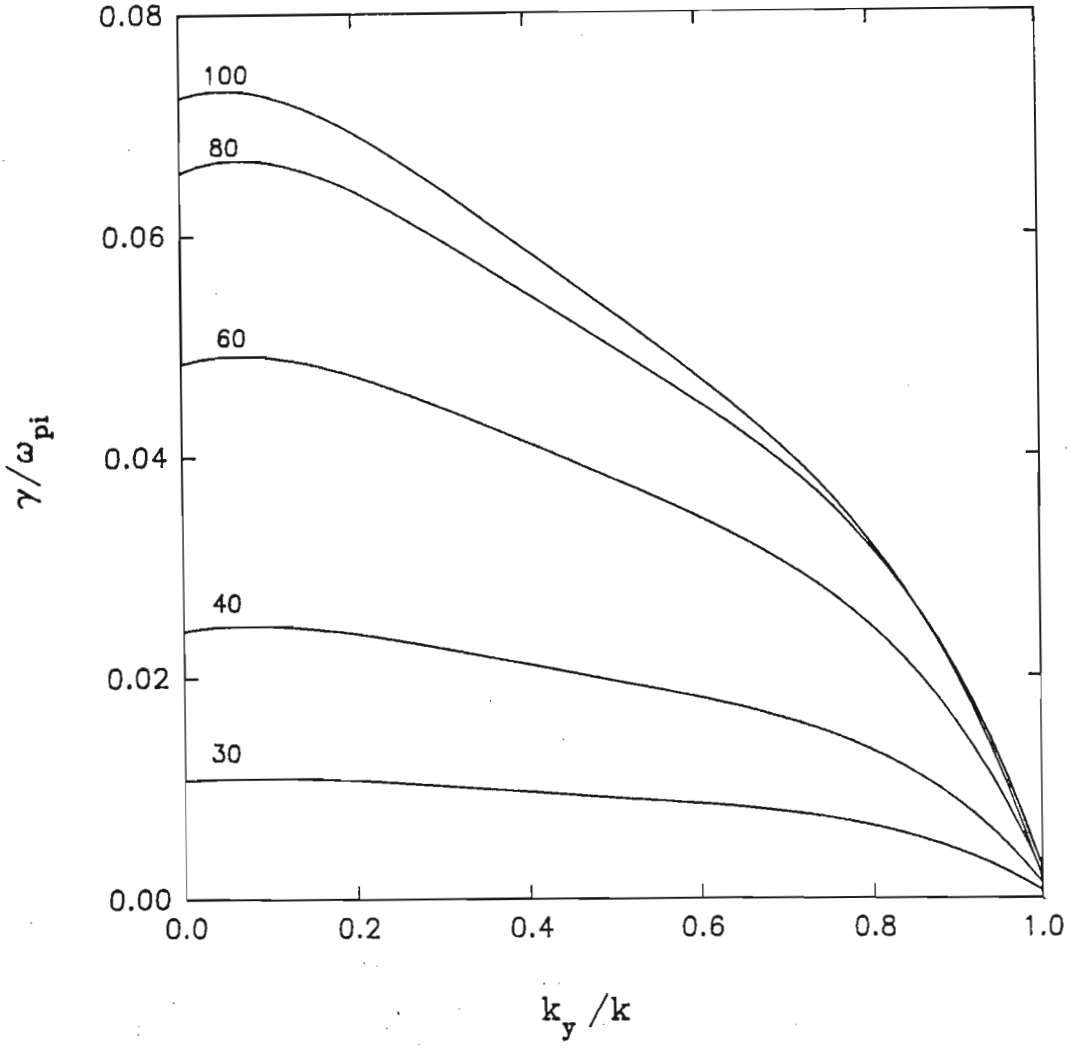

Figure 4.2: Normalized growth rate versus k_y/k with fixed parameters as for figure (4.1). The parameter labelling the curves is the ion beam speed, v_{dbz}.

The first term in equation (4.1) may be written as

$$kv_d \cos\theta$$

where θ is the angle between the velocity vector and the magnetic field. For $\theta = 0^o$ i.e. $k_y/k = 0.0$, the real frequency attains a maximum, which is consistent with the curves in figure (4.1). The threshold velocity for the slow ion-acoustic mode to have a real frequency is from equation (4.2) approximately equal to (for our parameters) $C_s/\sqrt{2} = \sqrt{1000}/\sqrt{2} = 22.3$, which is consistent with our results in figure (4.3).

4.3.2 The effect of increasing v_{dbz}

Figures (4.3) and (4.4) show the real frequency and growth rate curves as a function of the ion beam drift speed respectively. A calculation of the gradient of the curve in figure (4.3) yields the value 0.0095 which is almost equal to the chosen value for the fixed wavenumber, k=0.01. This is in agreement with equation (4.2), which for $k_y/k = 0$ and fixed k may be written as

$$\omega_r = mV_0 - C$$

which is a straight line with slope $m = k$. The curve also illustrates the lower threshold value of $V_0 = 22.2$ required for ω_r to be positive. From figure (4.4) it is seen that the growth rate maximizes at the normalized velocity of 100. In Gary and Omidi (1986) a similar result was obtained for the ion-ion acoustic instability. For our parameters, the maximum is at approximately three times the hot electron sound speed.

At a velocity of $v_{dbz} = 182C_s$, we find a sharp transition from the slow ion-acoustic mode to a simple beam instability. The real frequency and growth rate versus drift

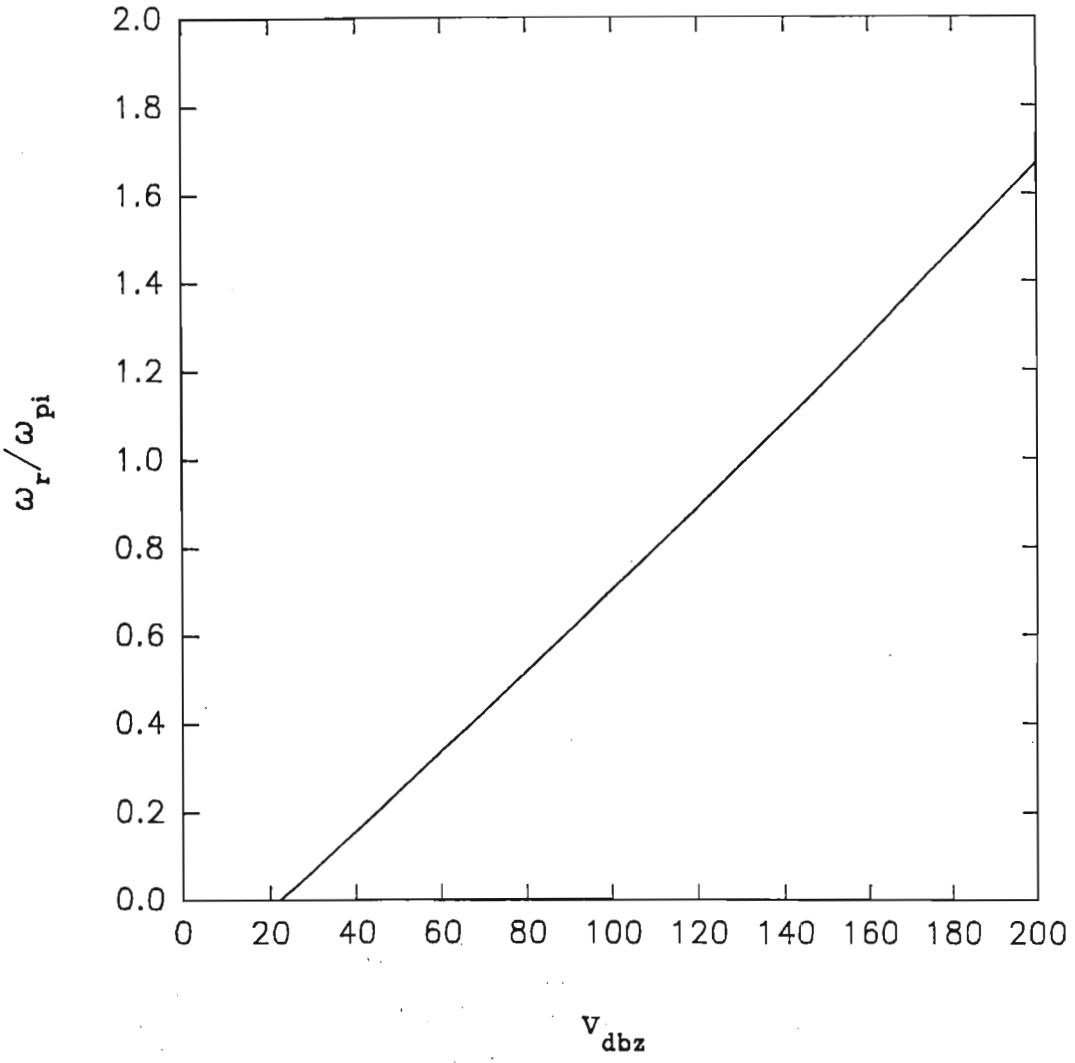

Figure 4.3: Normalized real frequency versus ion-beam speed, v_{dbz} for the slow beam ion-acoustic wave. Here $k_y/k = 0.0$ and other fixed parameters are as for figure (4.1).

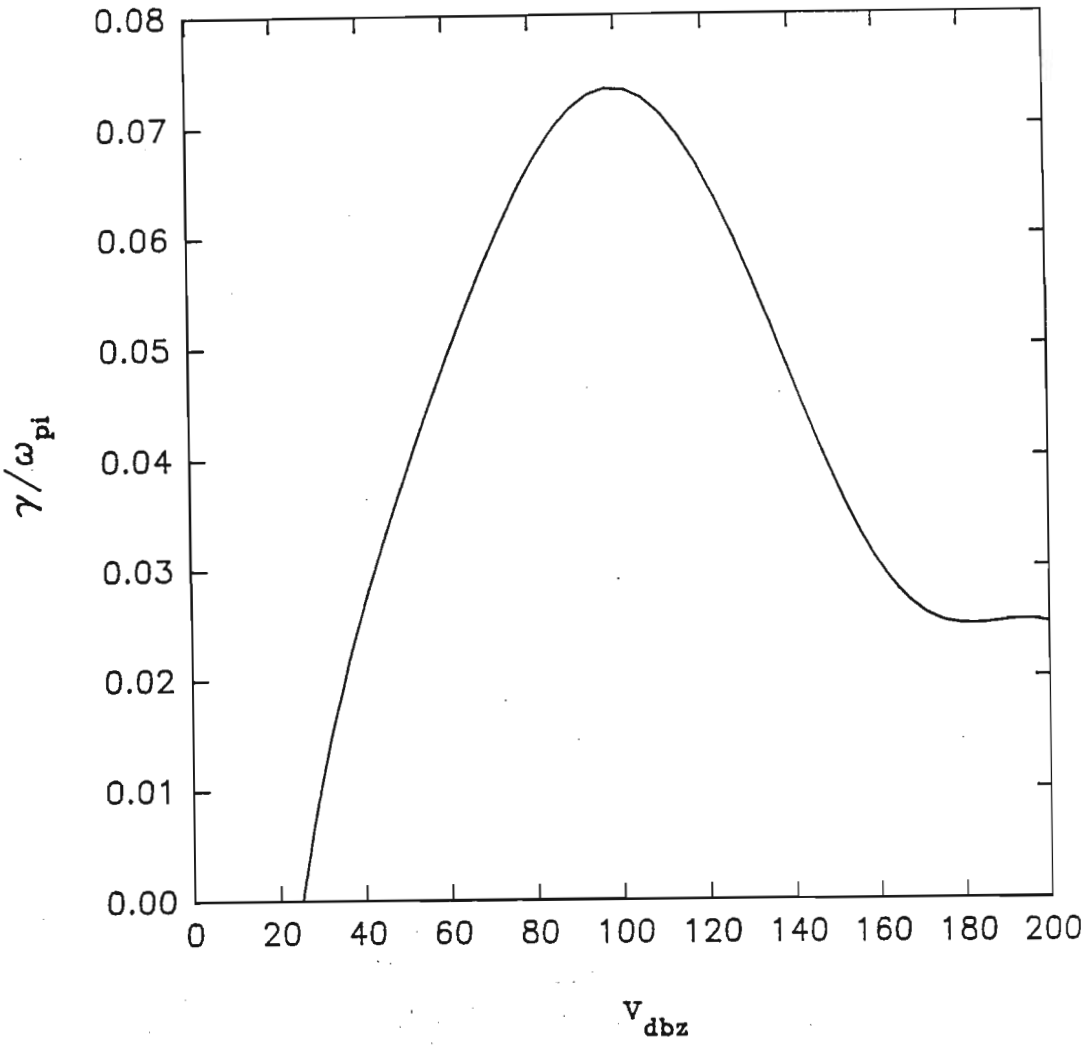

Figure 4.4: Normalized growth rate versus ion-beam speed, v_{dbz}, for the slow beam ion-acoustic wave. Here $k_y/k = 0.0$ with other fixed parameters as in figure (4.1).

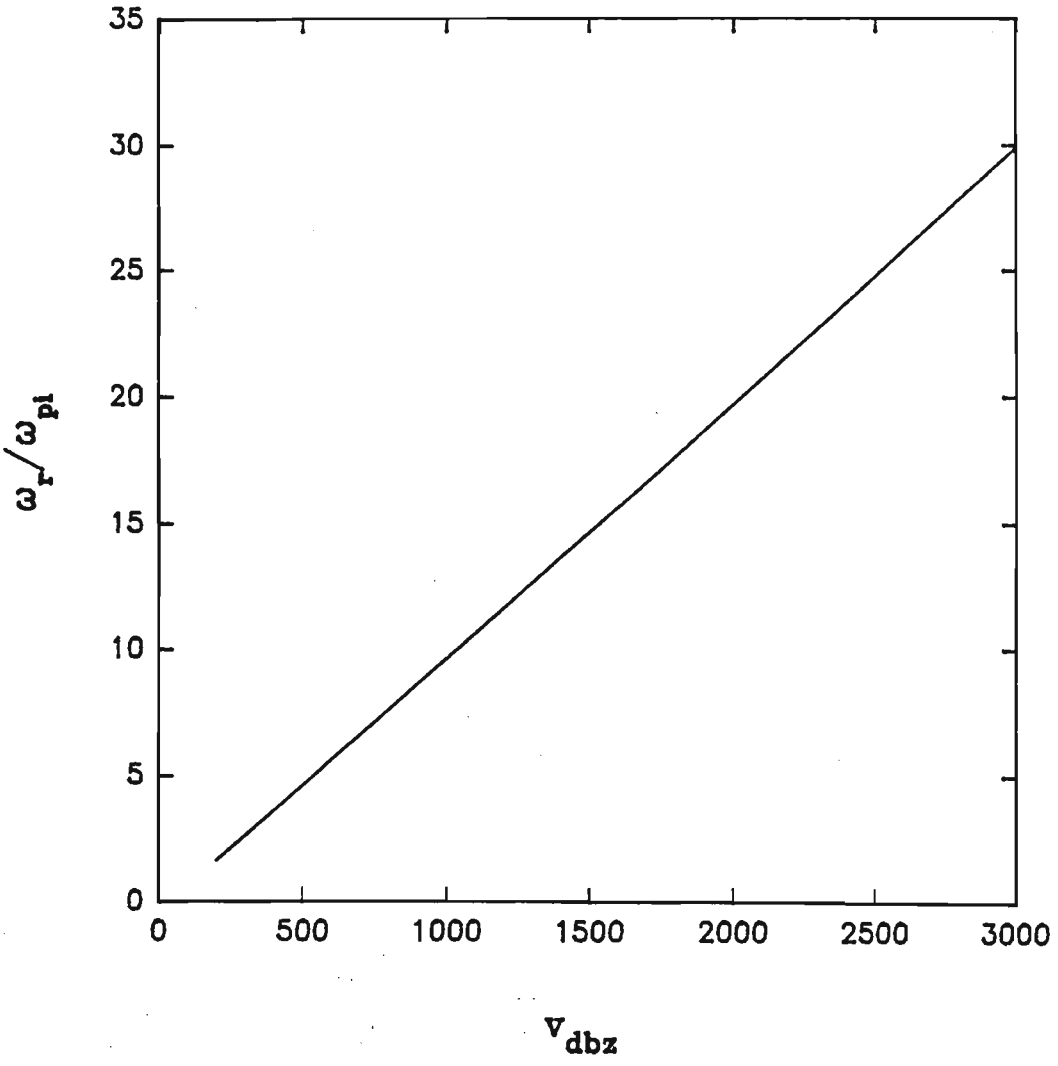

Figure 4.5: Normalized real frequency versus ion-beam speed, v_{dbz}, for the ion-beam instability at drifts $> 200C_s$. Here $k_y/k = 0.0$ and other fixed parameters are as in figure (4.1).

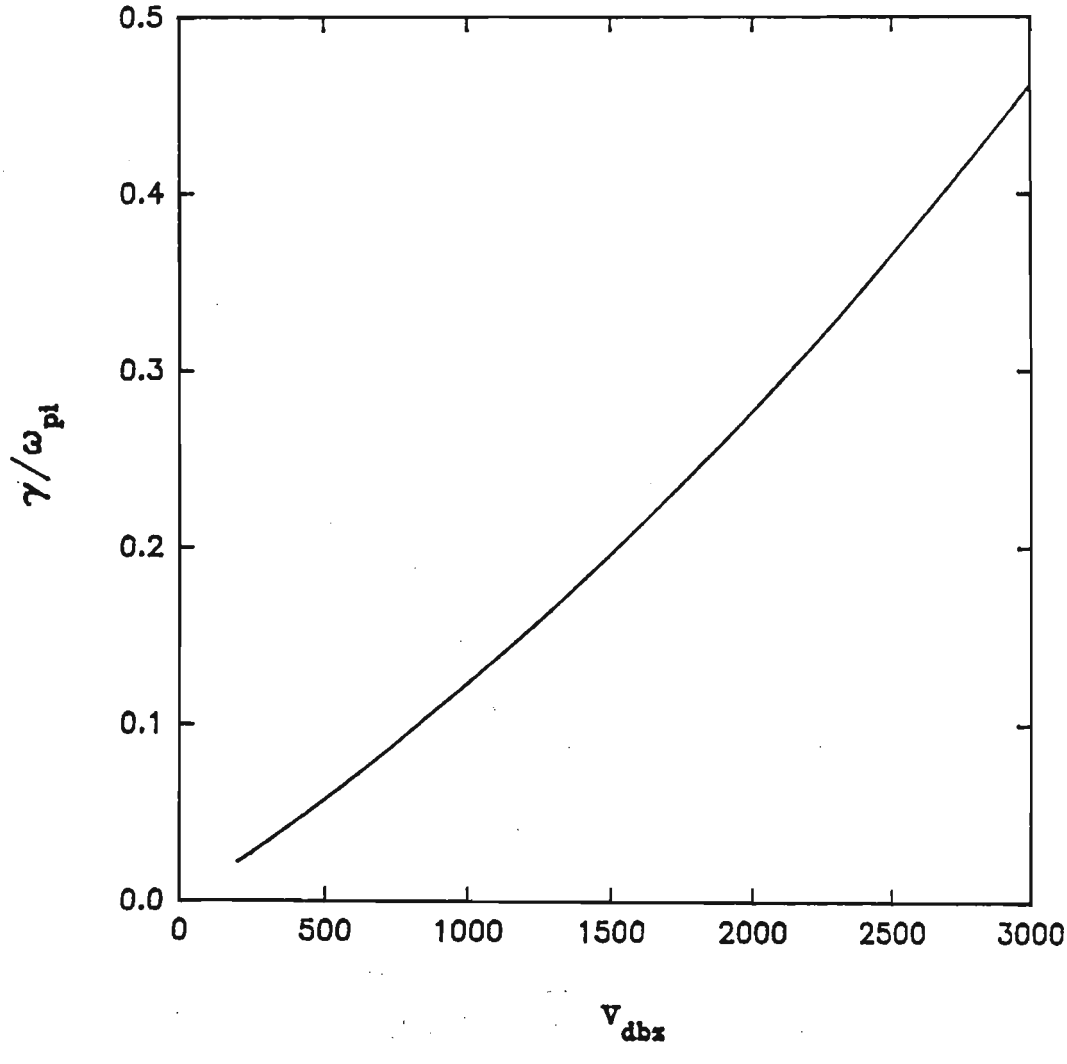

Figure 4.6: Normalized growth rate versus ion-beam speed, v_{dbz}, for the ion-beam instability at drifts $> 200\ C_s$. Here $k_y/k = 0.0$ and other fixed parameters are as in figure (4.1).

speed curves are shown in figures (4.5) and (4.6). It is seen that this instability propagates at the phase velocity:

$$v_\phi = \frac{\omega_r}{k} = V_0,$$

for a broad range of beam speeds, with the growth rate increasing with beam speed (figure (4.6)).

4.3.3 The effect of varying the wavenumber, k

The effect of varying the wavenumber was examined at a drift speed of $v_{dbz} = 100C_s$ for fixed propagation angles of $0°, 45°$ and $90°$. We note from the above that for the particular choice of v_{dbz}, the instability is identified as the IAI. The real frequency and growth rate curves are plotted in figures (4.7) and (4.8) respectively. The parameter labelling the curves is k_y/k. It is seen that for parallel propagation, the instability is present over a broad region in k-space. This is expected since the term $kv\cos\theta$ is a maximum at $0°$. The strong θ - dependence of the ion-acoustic mode is also evident. The maximum growth rate, $(\gamma/\omega_{pi})_{max}$, decreases significantly for angles of propagation oblique to $\mathbf{B_0}$. This is in agreement with the features of the slow ion-acoustic wave. This is not a surprising result since from figure (4.2) we see that γ/ω_{pi} is a maximum for propagation along $\mathbf{v_{dbz}}$, when resonance is a maximum. Therefore, at almost perpendicular propagation ($k_y/k = 0.99$) the wave "absorbs" very little energy from the beam. Thus the instability is weak.

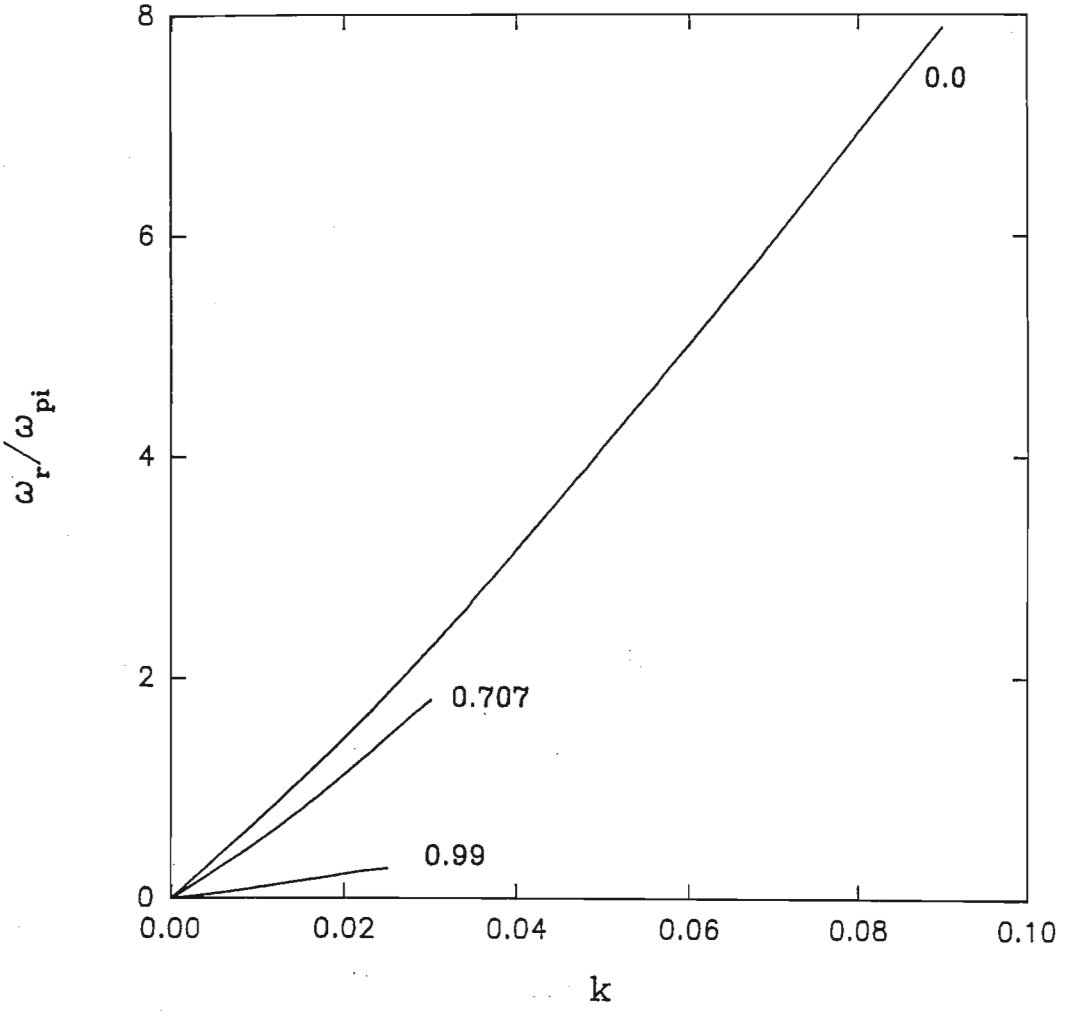

Figure 4.7: Normalized real frequency as a function of wavenumber, k, for k_y/k = 0.0, 0.707 and 0.99. Here , $v_{dbz} = 100C_s$, and other fixed parameters are as for figure (4.1).

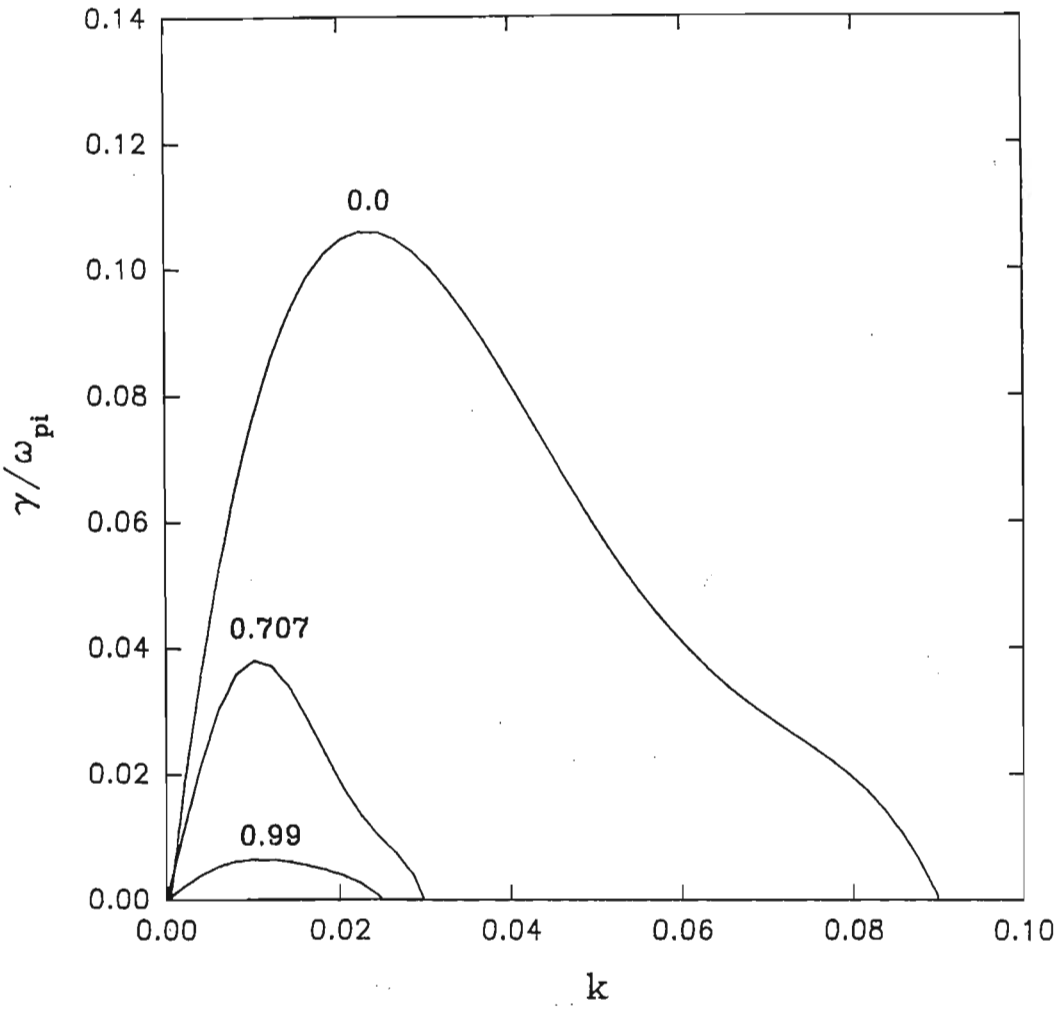

Figure 4.8: Normalized growth rate as a function of wavenumber, k, for the parameters of figure (4.7)

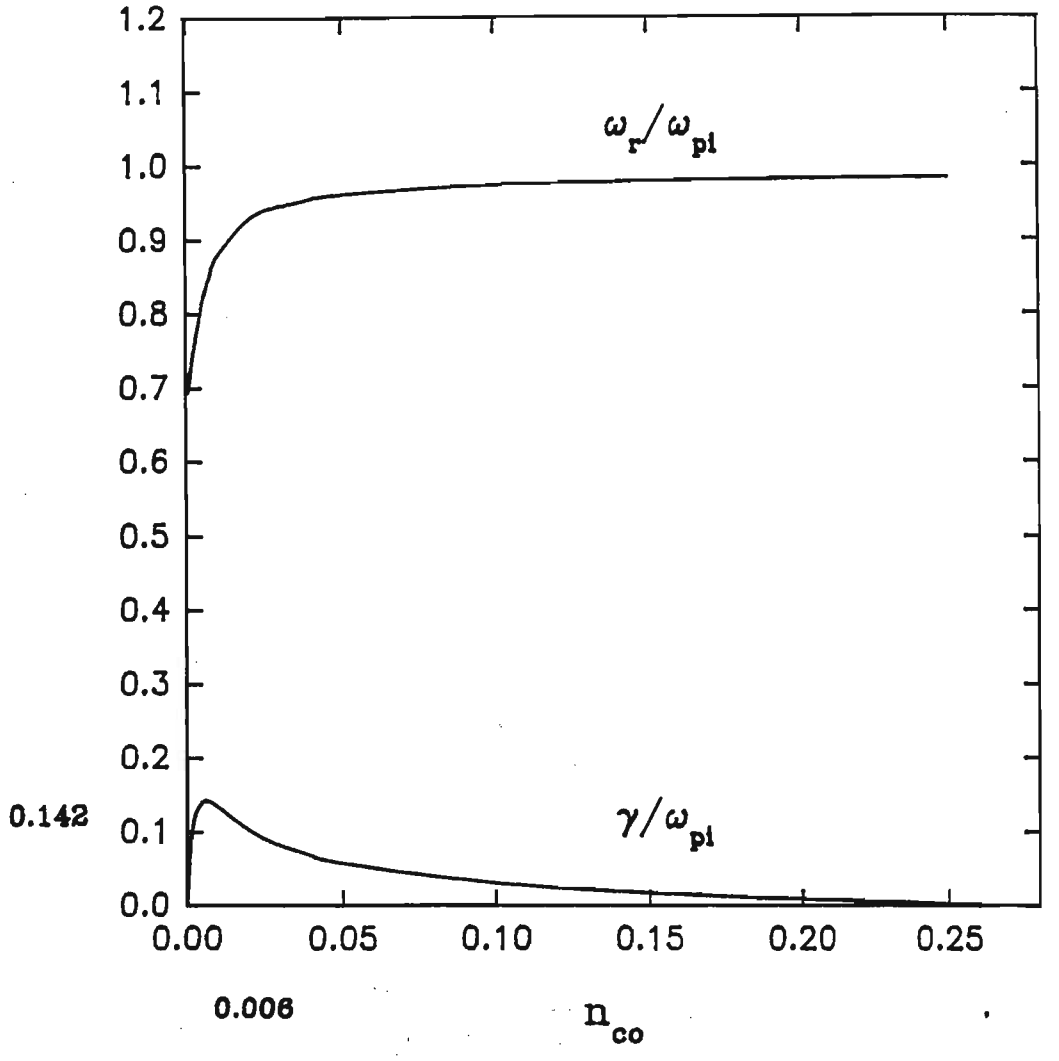

Figure 4.9: Normalized real frequency and growth rate as a function of the cold electron density, n_{co}, for $k_y/k = 0.0$ and beam velocity, $v_{dbz} = 100C_s$. The maximum growth rate is 0.142 at a density of 0.006. Other fixed parameters are as for figure (4.1).

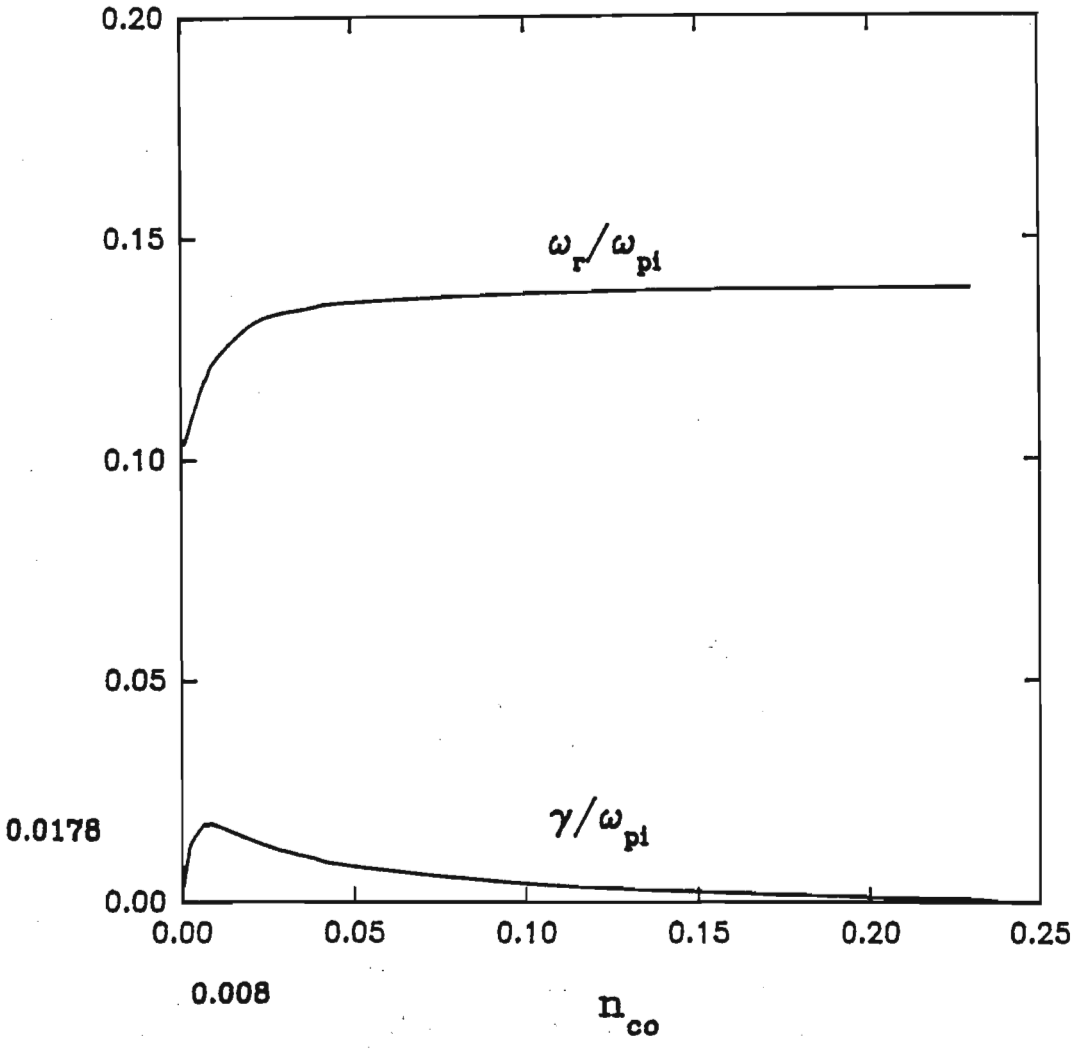

Figure 4.10: Normalized real frequency and growth rate as a function of the cold electron density, n_{co}, for $k_y/k = 0.99$ and beam velocity, $v_{dbz} = 100C_s$. The maximum growth rate is 0.0178 at a density of 0.008. Other fixed parameters are as for figure (4.1).

4.3.4 The effect of varying the cold background electron density, n_{co}

Although constituting a small fraction of the total particle density, in Lakhina(1993), the stationary background electrons were found to be essential for the generation of the ion beam instability. We examined the effect of varying this cold electron density on the ion-acoustic instability with a beam drift of $v_{dbz} = 100C_s$ and k=0.01. For parallel propagation where the real frequency and growth rate were found earlier to be a maximum, the results are shown in figure (4.9). Investigations have been done by Bergmann and Lotko(1986), Bergmann et.al(1988) and others on the ion-acoustic instability in the absence of cold stationary electrons. In their investigations, they assumed two ion species. The relative drifts in the ion-ion plasma allowed for the excitation of these modes.

Our results indicate that the plasma is unstable in the absence of the cold electrons (i.e. when $n_{co} = 0$). However, as we increase n_{co}, we find that there is an optimum value at which the instability growth rate attains a maximum. This is illustrated in the growth rate curve in figure (4.9) by the sharp rise in γ/ω_{pi} to a maximum value of 0.142 for $n_{co} = 0.006$. As n_{co} is increased further, we see that positive growth ceases at n_{co} beyond 0.260. This is most probably due to Landau damping. At near perpendicular propagation, the instability, as seen in earlier results, is weak. Still, the behaviour in response to a change in the cold electron density is similar to that found for parallel propagation (refer to figure (4.10)). In this case, the maximum for the growth rate is $(\gamma/\omega_{pi})_{max} = 0.0178$ at a density of $n_{co} = 0.008$.

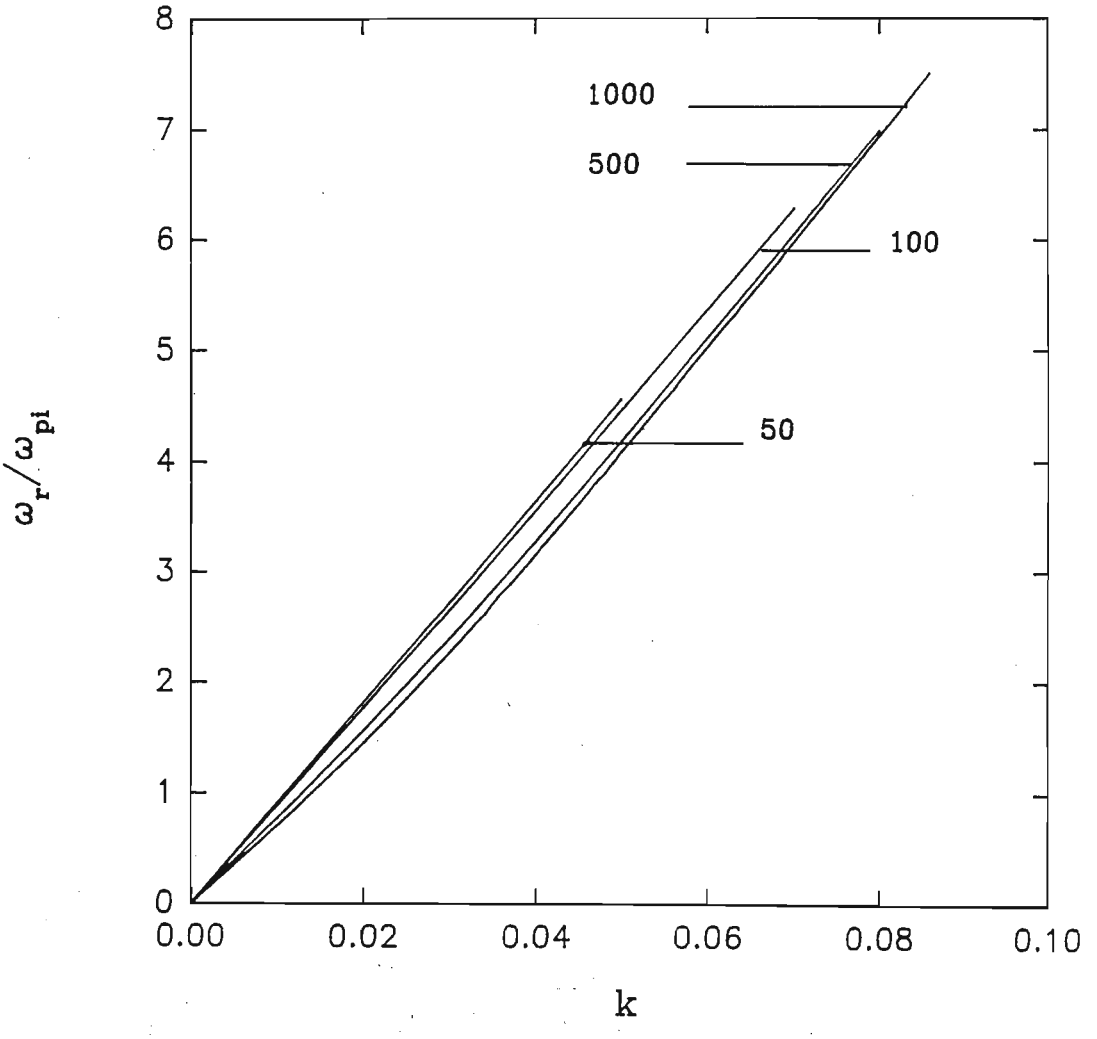

Figure 4.11: Normalized real frequency as a function of the normalized wavenumber, k. The parameter labelling the curves is the hot electron temperature, T_h/T_c. Here $k_y/k = 0.0$ and the beam velocity $v_{dbz} = 100C_s$. Other fixed parameters are as for figure (4.1).

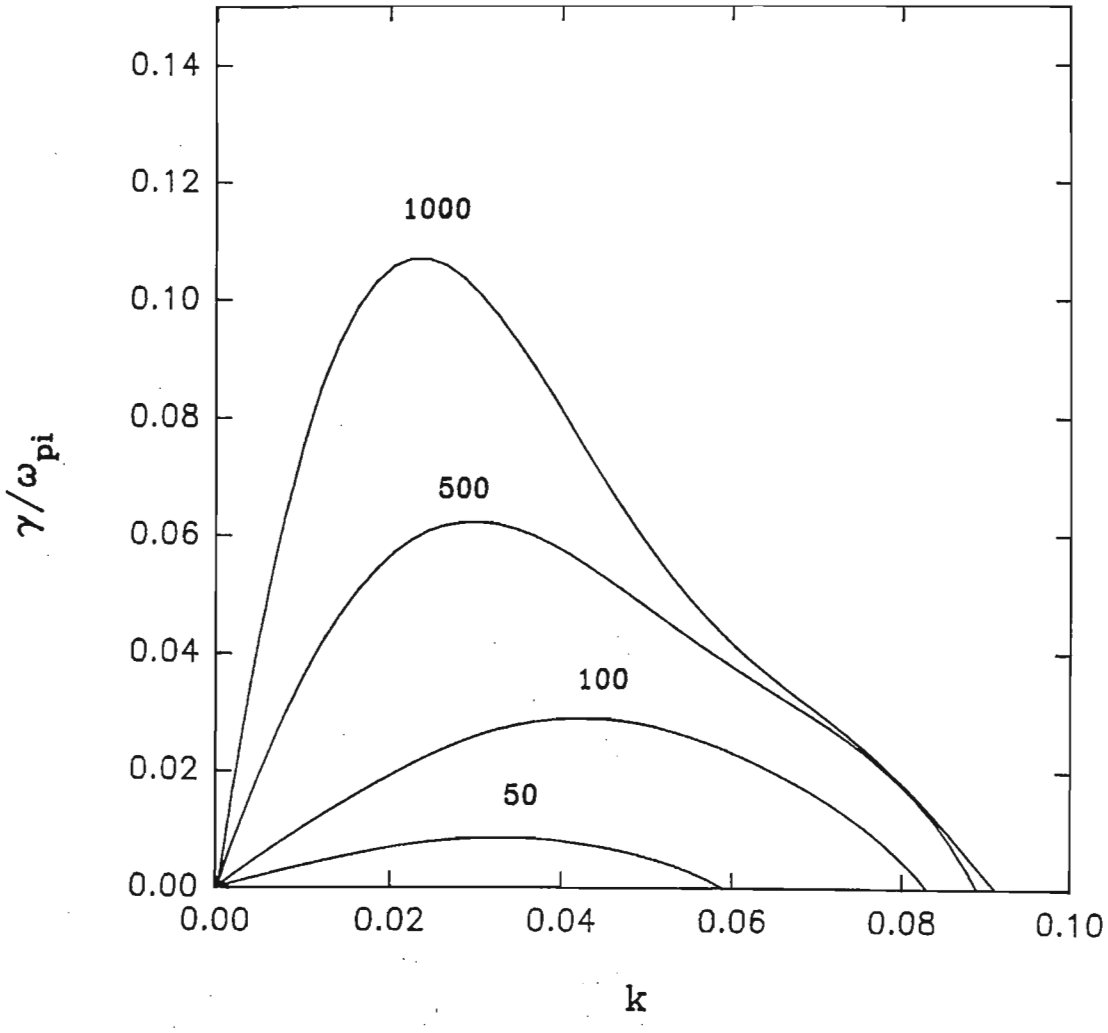

Figure 4.12: Normalized growth rate as a function of the normalized wavenumber, k, for the parameters of figure (4.11). The parameter labelling the curves is the hot electron temperature, T_h/T_c.

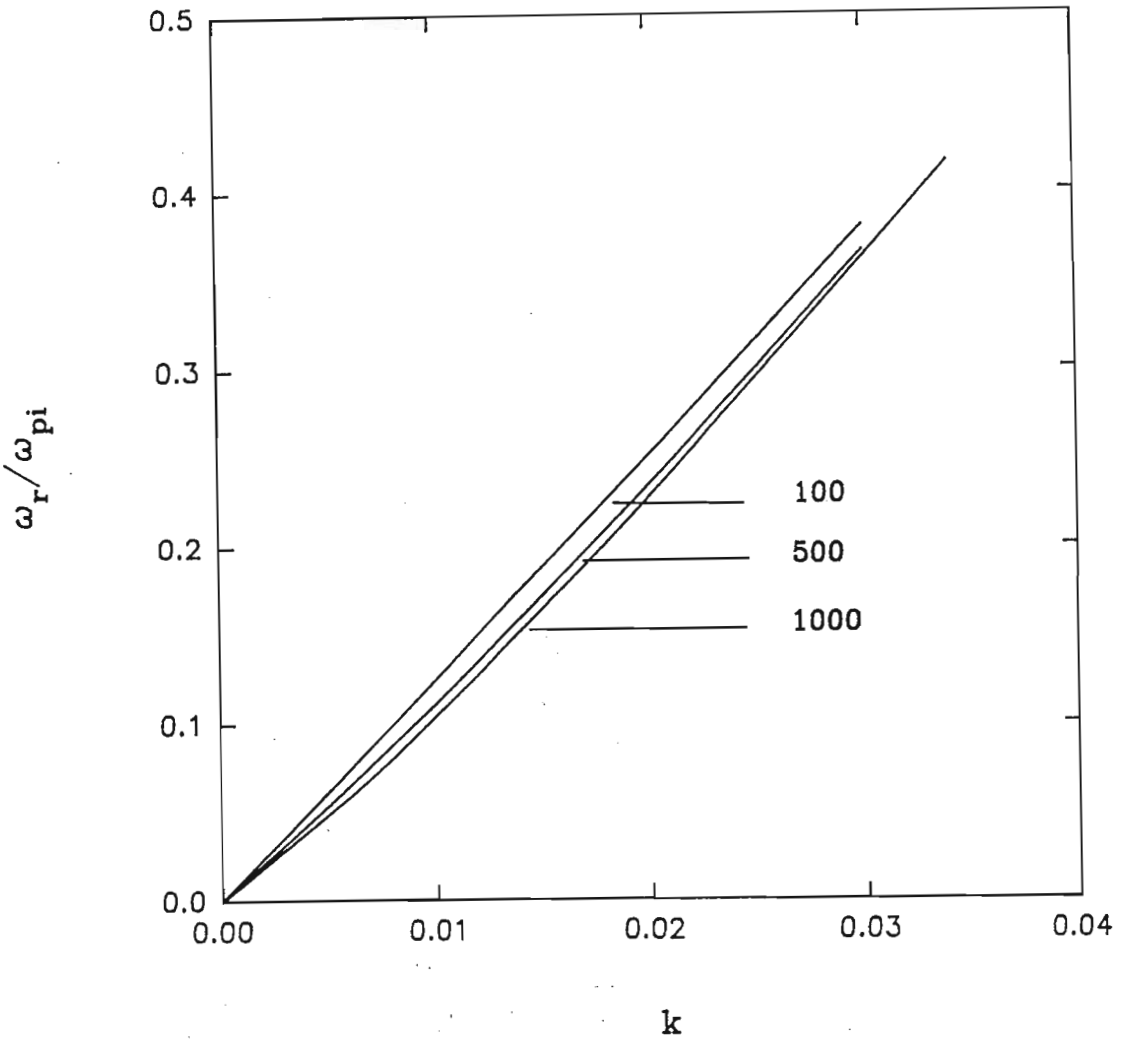

Figure 4.13: Normalized real frequency as a function of the normalized wavenumber, k. The parameter labelling the curves is the hot electron temperature T_h/T_c. Here $k_y/k = 0.99$ and the beam velocity, $v_{dbz} = 100C_s$. Other fixed parameters are as for figure (4.1).

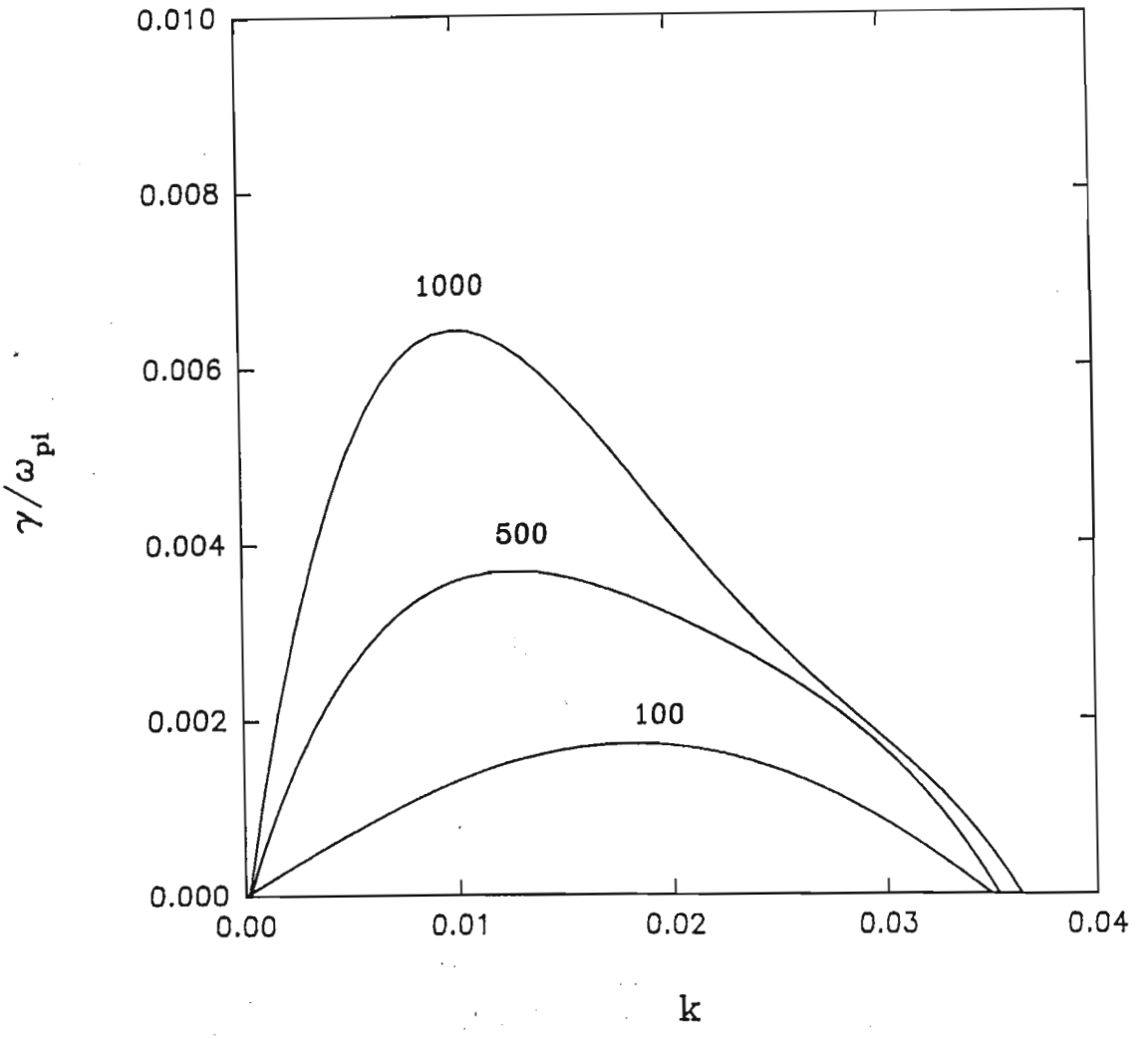

Figure 4.14: Normalized growth rate as a function of the normalized wavenumber, k, for the parameters of figure (4.13). The parameter labelling the curves is the hot electron temperature, T_h/T_c.

4.3.5 The effect of the hot electron temperature, T_h/T_c

Next we considered the effect of the hot electron temperature on the ion- acoustic instability. For these results the beam temperature was set at $T_b/T_c = 10$. The real frequency and growth rate curves for $k_y/k = 0.0$ are shown in figures (4.11) and (4.12) respectively, while for $k_y/k = 0.99$ the curves are shown in figures (4.13) and (4.14). The parameter labelling the curves is temperature. We find that as θ increases from 0^o to 90^o the lower temperature threshold cut off of the instability increases. Both figures (4.12) and (4.14) show increased growth rate for higher temperatures. Increasing the temperature of a species has the effect of increasing the thermal motions of the particles. For the ion-acoustic wave, thermal motion of the electrons is a necessary condition for the wave to exist. It is seen that the maximum for each value of T_h/T_c, at parallel (to $\mathbf{B_0}$) propagation angle, is higher than those for near perpendicular propagation. This is consistent with the results found in the k_y/k variation curves studied in section (4.1). We also find that for a fixed T_h/T_c, the k-value for $(\gamma/\omega_{pi})_{max}$ shifts to lower k as k_y/k increases. For a given propagation angle, the k-value for maximum growth rate shifts to the lower k region as the normalized temperature is increased above 100. The increase in growth rate with T_h may be associated with the decrease in electron Landau damping. The slow beam ion acoustic wave "sees" a negative slope $(\partial f_{eh}/\partial v_z)$ of the hot electron velocity distribution function $f_{eh}((v_z))$. As T_h increases, $f_e((\mathbf{v}))$ "flattens" with $(\partial f_{eh}/\partial v_z)$ decreasing. Since the associated Landau damping is proportional to $(\partial f_{eh}/\partial v_z)$, it also decreases, thereby causing an increase in the net growth rate γ/ω_{pi}.

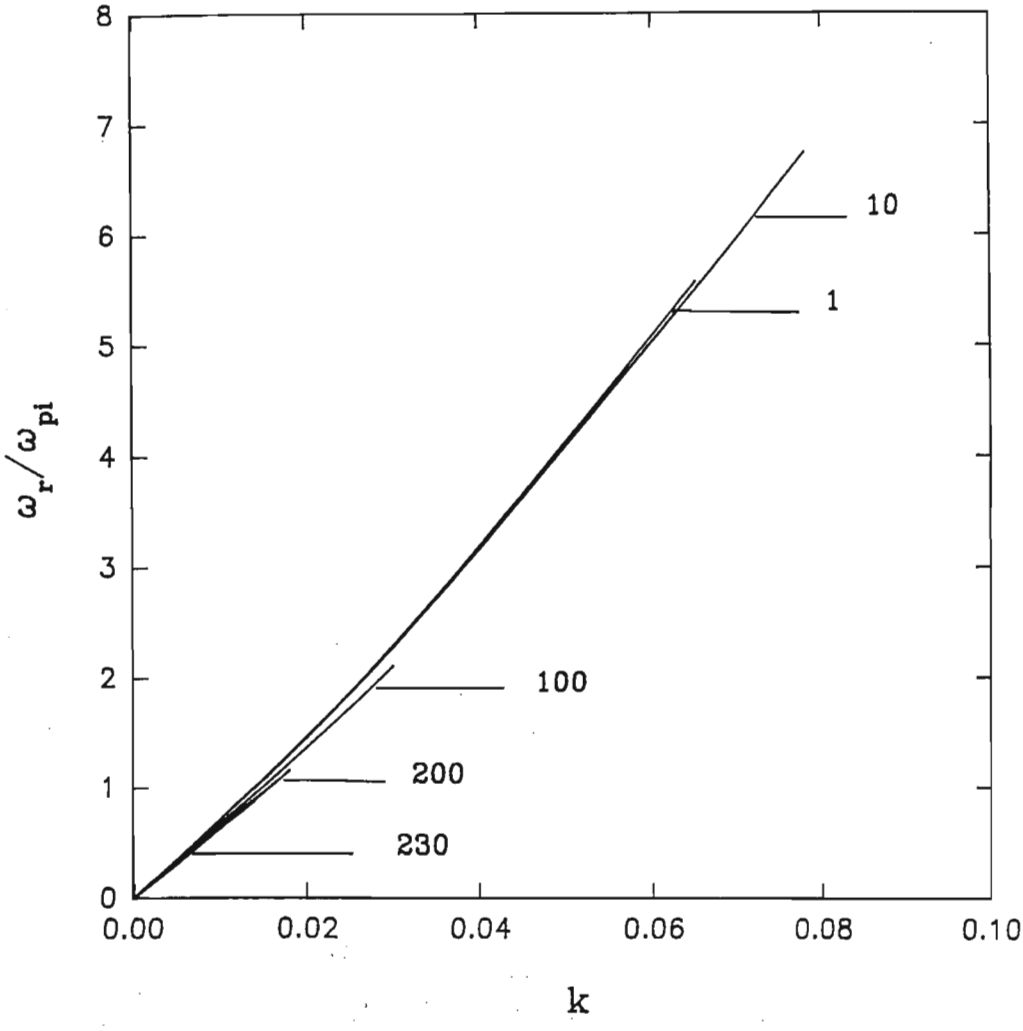

Figure 4.15: Normalized real frequency as a function of the normalized wavenumber, k. The parameter labelling the curves is the ion beam temperature, T_b/T_c. Here k_y/k = 0.0 and the beam velocity, $v_{dbz} = 100C_s$. Other fixed parameters are as for figure (4.1).

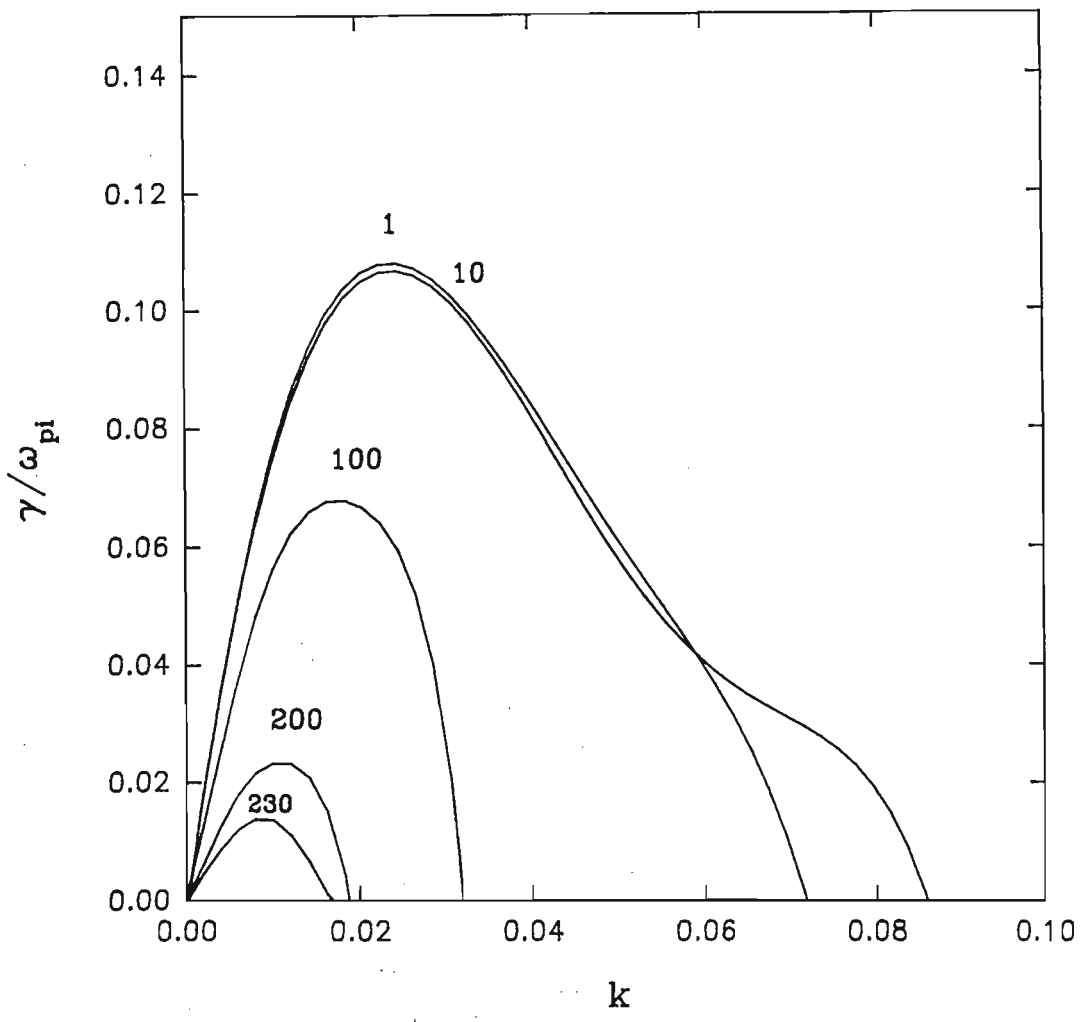

Figure 4.16: Normalized growth rate as a function of the wavenumber, k, for the parameters of figure (4.15). The parameter labelling the curves is the ion beam temperature, T_b/T_c.

4.3.6 The effect of the ion beam temperature

As mentioned in the introduction, the presence of hot ion beams have been observed in the auroral acceleration region. We examine in this section the effect of the ion beam temperature on the instability. For $k_y/k = 0.0$, the temperature of the hot electron component is fixed at $T_h/T_c = 1000$ and the instability dependence on increasing ion beam temperature is studied.

Raising the ion beam temperature has the effect of considerably lowering the maximum growth for the k-variation curves in figures (4.15) and (4.16). This is characteristic of the ion-acoustic instability for which a drifted Maxwellian is assumed. The condition $T_e/T_b >> 1$ is necessary to excite the mode, hence we find that as T_b is increased, the instability weakens. It was found that for the chosen fixed parameters, no positive growth was possible when $T_b > 230T_c$. Also, we find that for a higher temperature, the maximum growth shifts to a lower-k value and the range of k-values for positive growth decreases significantly.

The reduction in γ/ω_{pi} as T_b/T_c increases may be explained as follows: Since the slow-beam ion acoustic wave sees a positive slope for the ion beam velocity distribution, $f_b(v_z)$, as T_b increases, the "flattening" of $f_b(v_z)$ reduces $\partial f_b/\partial v_z$. Hence the inverse ion Landau damping decreases, thereby reducing the net growth rate.

4.4 The modified two-stream instability(MTSI)

4.4.1 The appearance of the MTSI

Figures (4.17) and (4.18) depict the real frequency and growth rate versus k_y/k curves for the two modes that were found to be present at the normalized drift velocity

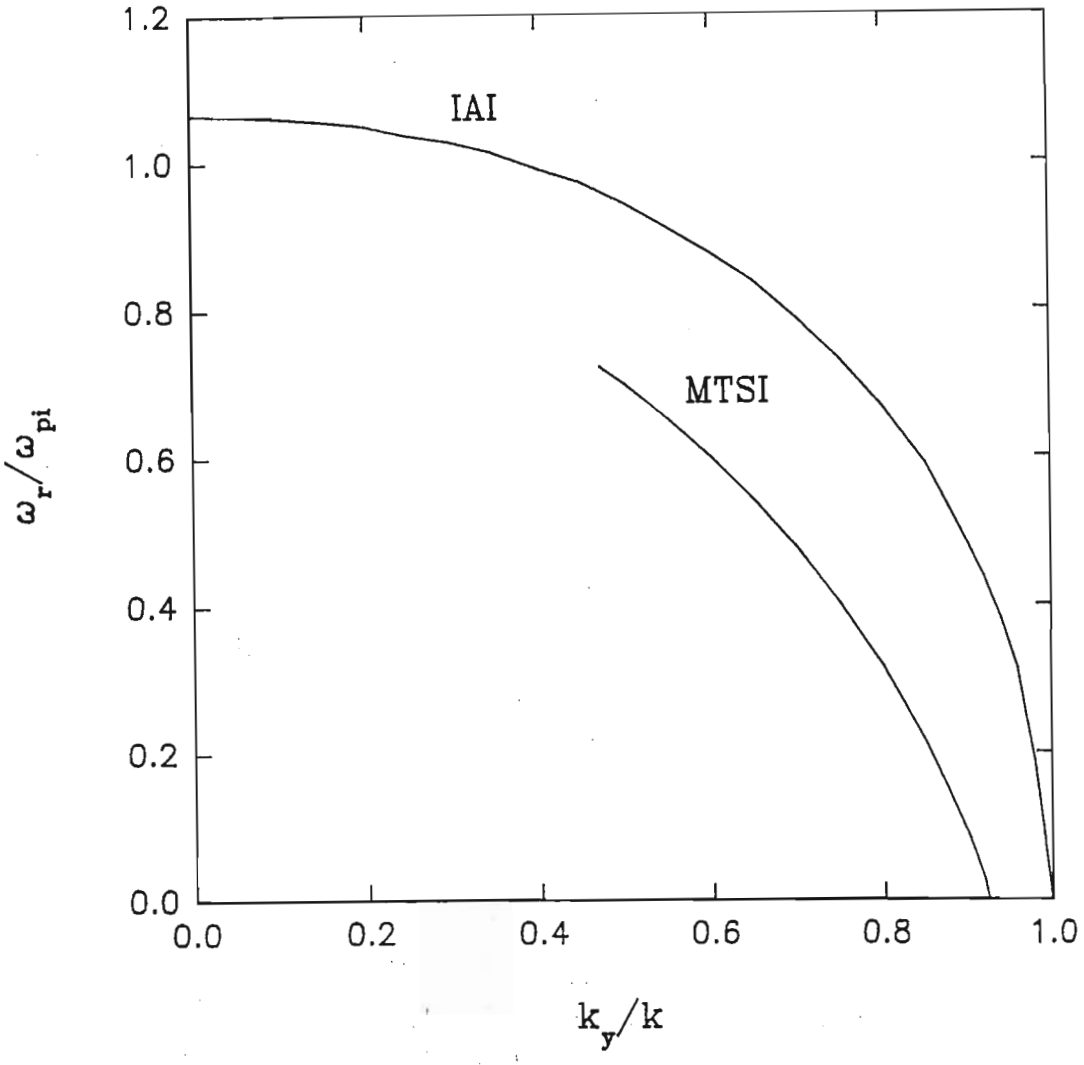

Figure 4.17: Normalized real frequency as a function of k_y/k for the IAI and the MTSI at ion beam speed, $v_{dbz} = 140$ and k= 0.01. Other fixed parameters are as for figure (4.1).

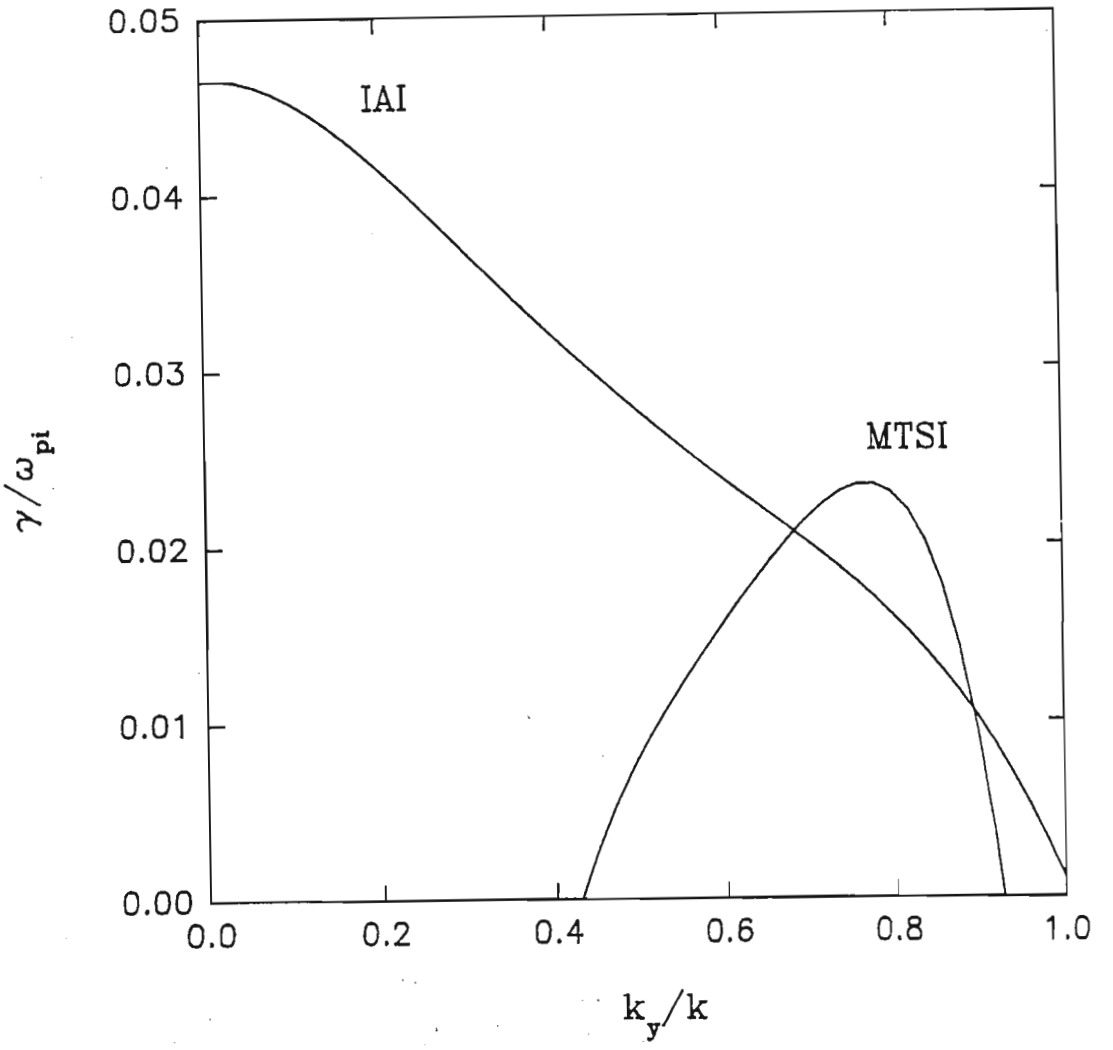

Figure 4.18: Normalized growth rate as a function of k_y/k for the IAI and the MTSI at ion beam speed $v_{dbz} = 140$ and k= 0.01. Other fixed parameters are as for figure (4.1).

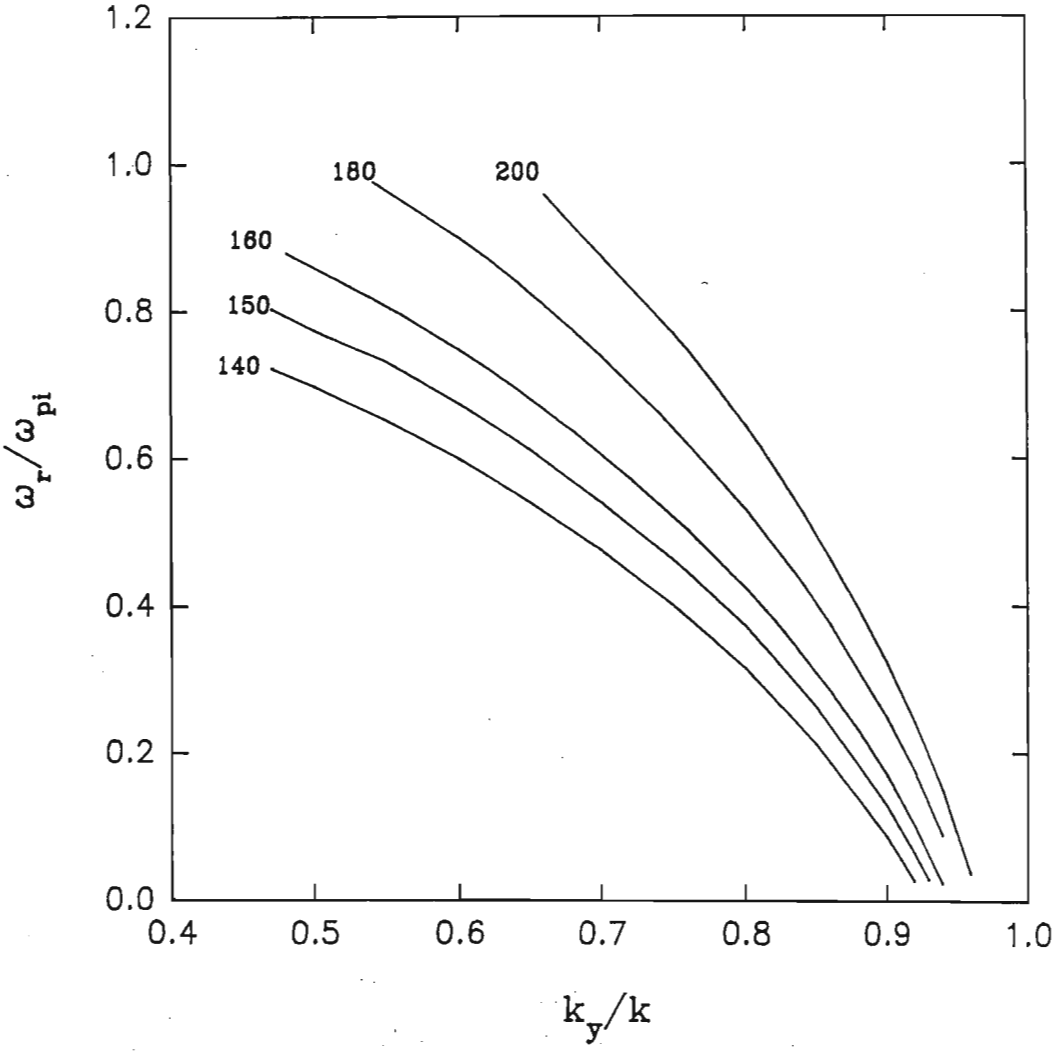

Figure 4.19: Normalized real frequency as a function of k_y/k for the MTSI. The parameter labelling the curves is the ion beam speed, v_{dbz}. Here k= 0.01 and other fixed parameters are as for figure (4.1).

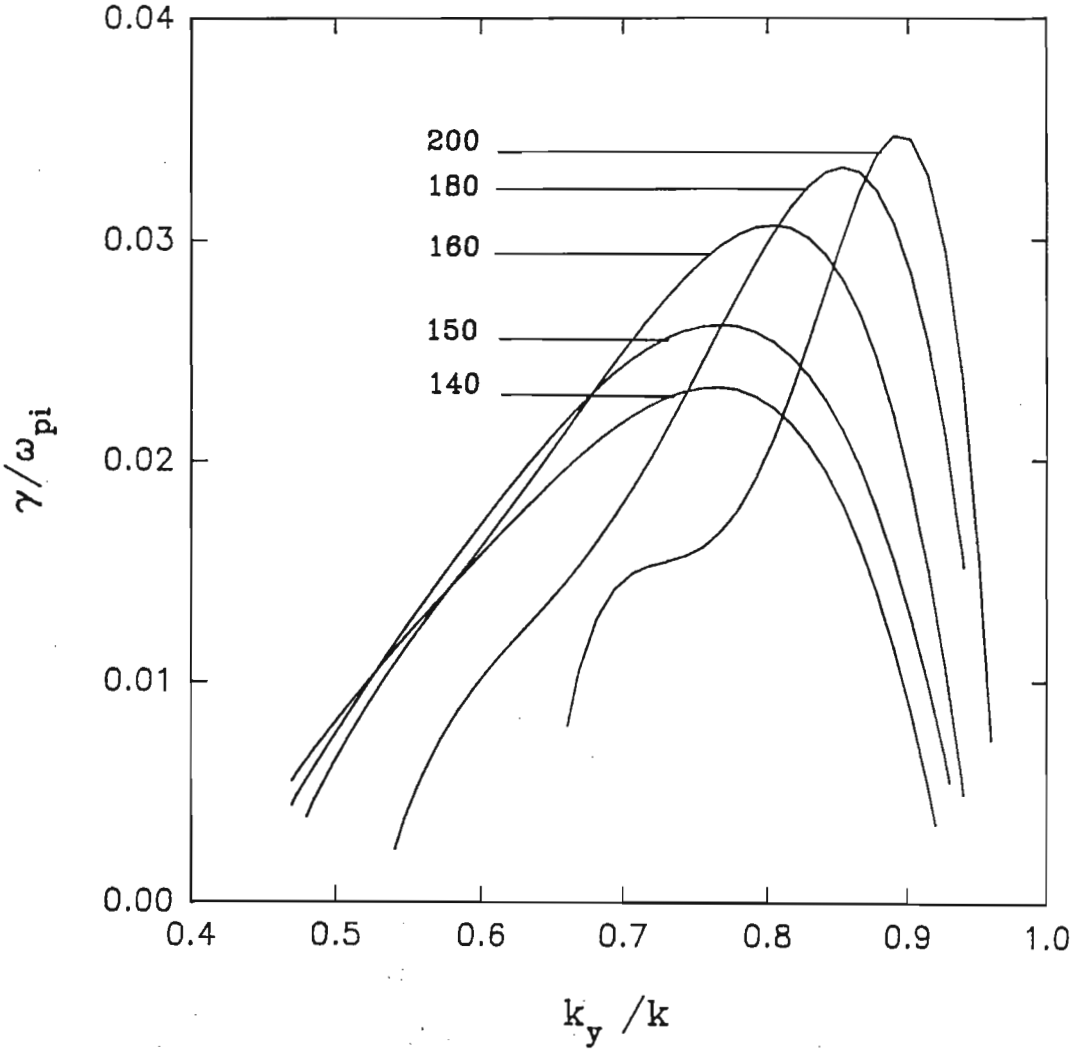

Figure 4.20: Normalized growth rate as a function of k_y/k for the MTSI. The parameter labelling the curves is the ion beam speed, v_{dbz}. Here k= 0.01 and other fixed parameters are as for figure (4.1).

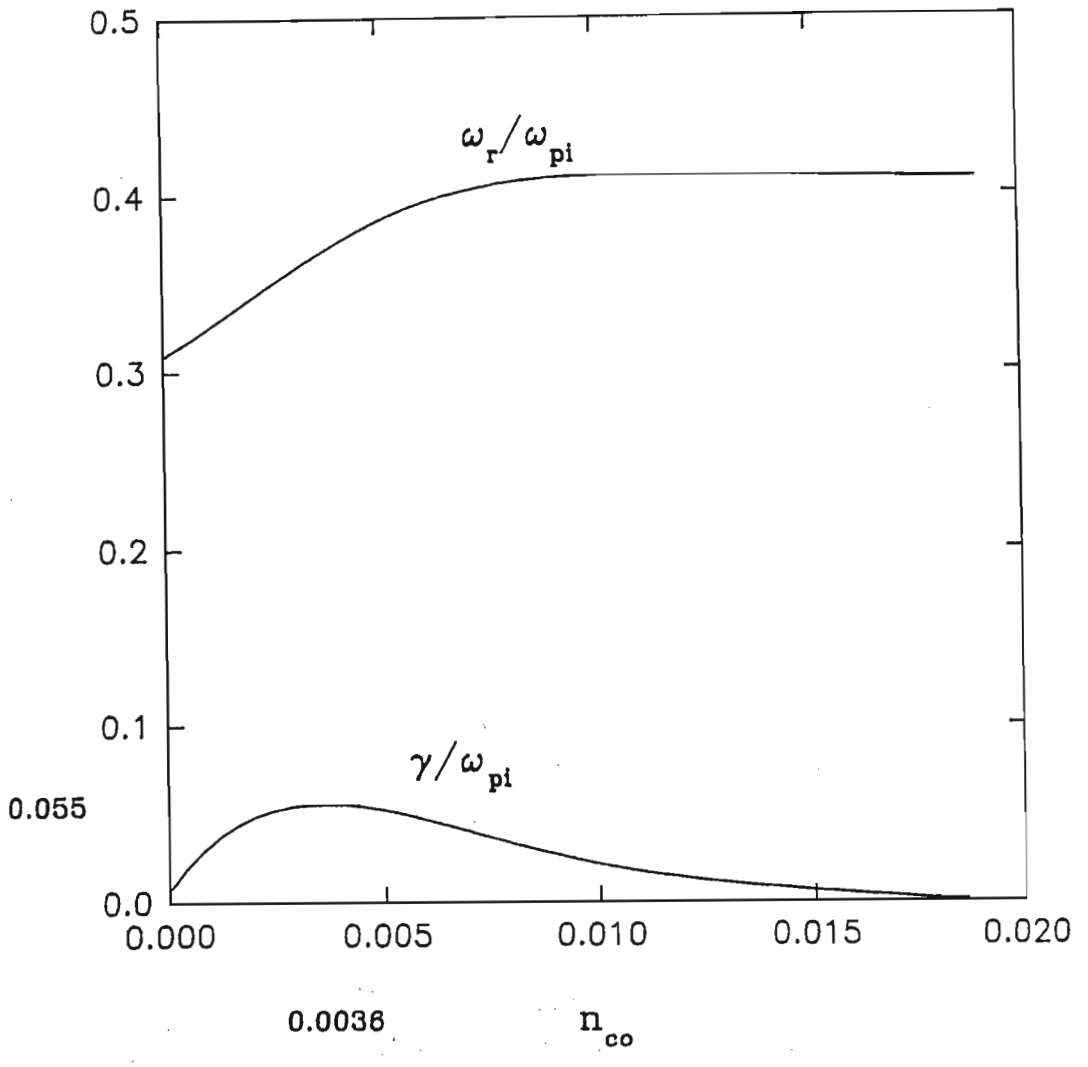

Figure 4.21: Normalized real frequency and growth rate as a function of n_{co} for the MTSI. Here $v_{dbz} = 200C_s$ and $k_y/k = 0.9$. Other fixed parameters are as for figure (4.1).

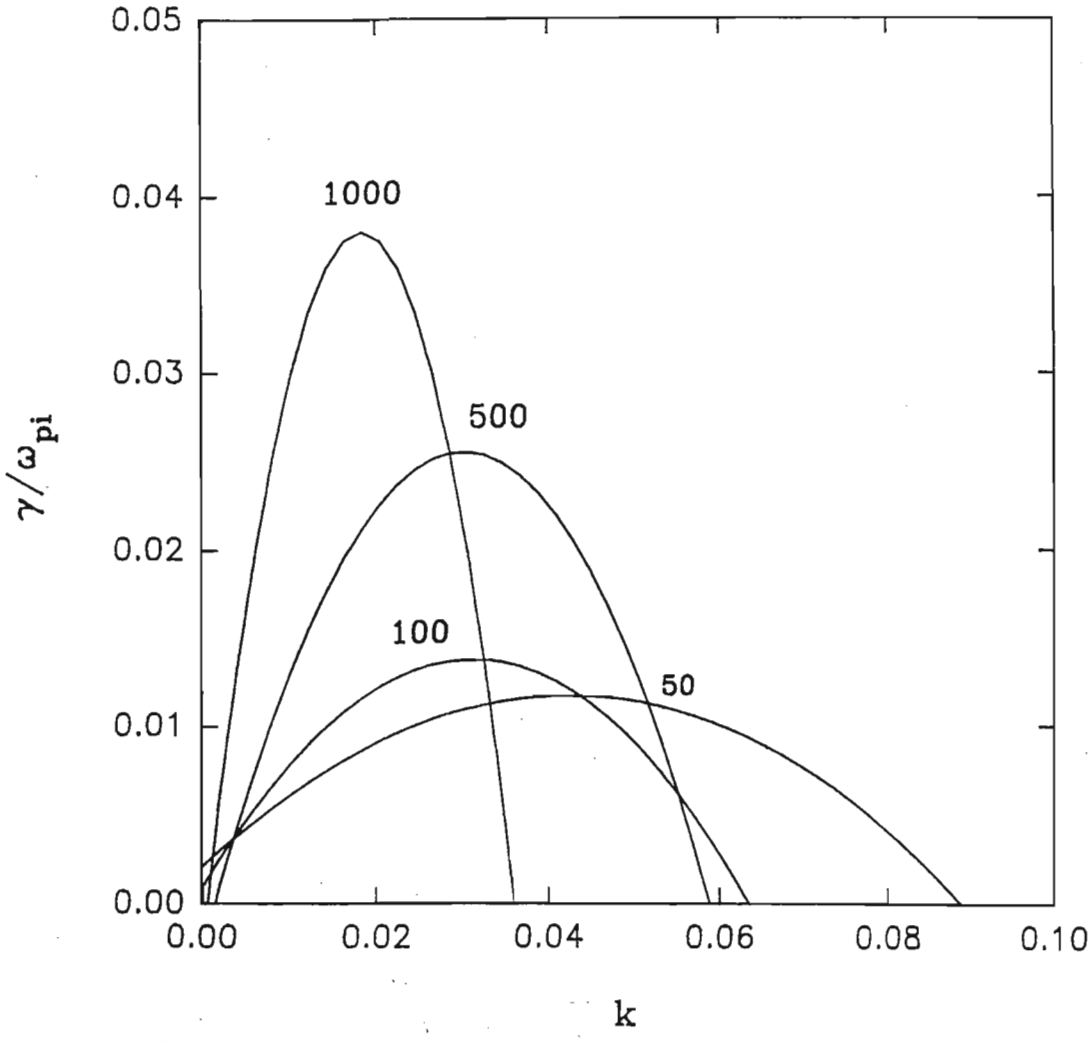

Figure 4.22: Normalized growth rate as a function of k for the MTSI. The parameter labelling the curves is the normalized hot electron temperature, T_h/T_c. Here $v_{dbz} = 200C_s$ and $k_y/k = 0.9$. Other fixed parameters are as for figure (4.1).

$v_{dbz} = 140$. We note the drop in the growth rate of the ion acoustic mode with k_y/k, which is consistent with figure (4.2).

The second mode appears at oblique angles of propagation, at the normalized drift speed of $v_{dbz} = 140C_s$, such that $k_y/k > 0.4$. The growth rate curve shows that the mode grows for increasing ion beam drift velocity. In order to identify the mode, a parameter variation study was made.

4.4.2 Results of k_y/k variation

Figures (4.19) and (4.20) show the real frequency and growth rate curves for the second mode at normalized drifts of 140, 150, 160, 180 and 200.

The features of this instability is consistent with that of a modified two-stream instability that arises from the relative drift of the plasma species . This is a well known electrostatic plasma instability for propagation oblique to $\mathbf{B_o}$. When the relative drift is between ions and electrons, the instability is called a Buneman instability. Two stream instabilities have been investigated by Bergman et.al.(1988) in the auroral acceleration region. It was found that for the Buneman instability, the excited wave has the phase velocity of the slow mode of an ion beam instability. $v_{db} > C_s$ was found to be a condition for the instability. This low-frequency instability has been found to propagate in a narrow cone about the perpendicular to the magnetic field, $\mathbf{B_0}$, (J.B. McBride et. al., 1972).

4.4.3 The effect of varying the cold background electron density, n_{co}

Figure (4.21) shows the real frequency and growth rate versus cold electron density, n_{co}, curves for the MTSI at the normalized drift velocity of $v_{dbz} = 200C_s$. For this plot, k= 0.01 and $k_y/k = 0.9$. We find here, as for the ion acoustic instability, an optimum value of the cold background species at which the instability growth rate attains a maximum. A maximum growth rate of $\gamma/\omega_{pi} = 0.055$ was found for $n_{co} = 0.0036n_o$.

4.4.4 The effect of the hot electron temperature, T_h/T_c

Figure (4.22) shows the growth rate versus normalized k curves for normalized hot electron temperatures T_h/T_b =50, 100, 500 and 1000. For these results, the drift velocity was also set to $v_{dbz} = 200C_s$, with $k_y/k = 0.9$ and $T_b/T_c = 10$. We note here also the increased growth rate for higher temperatures. As T_h/T_c increases significantly, $(\gamma/\omega_{pi})_{max}$ shifts to lower values of k.

Chapter 5

The effect of counter-streaming hot electrons

5.1 Introduction

In this chapter we examine the effect that the hot precipitating electrons, given a non-zero drift velocity, has on the instabilities studied in chapter 4. The electron drift is in the direction opposite to the magnetic field, **B**, and therefore opposite also to the ion beam drift velocity. A parameter variation study is made and the results compared with those of chapter 4 in which the hot electrons were taken to be stationary.

5.2 The ion acoustic instability

5.2.1 Variation of propagation angle, k_y/k

The ion acoustic instability was studied with the ion beam drift velocity, v_{dbz}, fixed at $100C_s$. Figures (5.1) and (5.2) show the real frequency, ω_r/ω_{pi}, and growth rate ,

γ/ω_{pi}, curves for the normalized electron drift velocities of 0 (i.e. stationary electrons), -50, -100, and -150. We observe in figure (5.1) that the real frequency response to the variation of electron drift velocity is not significant. This is to be expected since from equation (4.1), we note that for the slow ion acoustic instability, ω_r is a function of the ion drift velocity and not the electron drift velocity. This dependence on the ion drift velocity is clearly shown in figure (5.3) where, in this case, a significant increase in the real frequency, ω_r/ω_{pi} is seen. For $v_{dbz} = 100C_s$, $\omega_r/\omega_{pi} = 0.71$ while for $v_{dbz} = 150$, $\omega_r/\omega_{pi} = 1.18$ at $k_y/k = 0$. The decrease in the growth rate curve for the drift velocity, $v_{dbz} = 150$ in figure (5.4), is consistent with the results in chapter 4 where we found that γ/ω_{pi} has a maximum at $v_{dbz} = 100C_s$.

In figure (5.2) we observe that increasing the electron drift velocity results in a decrease in the growth rate. This may be understood in terms of the effect of electron Landau damping. The slow ion acoustic wave for which the ion beam distribution function attains a maximum at $v_{dbz} = 100C_s$, 'sees' the slope, $(\partial f_{eh}/\partial v_z)$, of the electron distribution function, $f_{eh}(v_z)$, increasing in magnitude as the electron velocity distribution shifts laterally in the $-v_z$ direction. Since electron Landau damping is proportional to $(\partial f_{eh}/\partial v_z)$, it also increases resulting in a drop in the growth rate.

5.2.2 The effect of varying the cold background electron density, n_{co}

With the ion beam drift velocity, $v_{dbz} = 100C_s$ and the electron drift velocity, $v_{dhz} = -100C_s$, the effect of varying the cold electron density was examined. The real frequency and growth rate curves depicted in figures (5.5) and (5.6) are similar to those of chapter 4, figures (4.9) and (4.10). In the presence of a non-zero hot electron

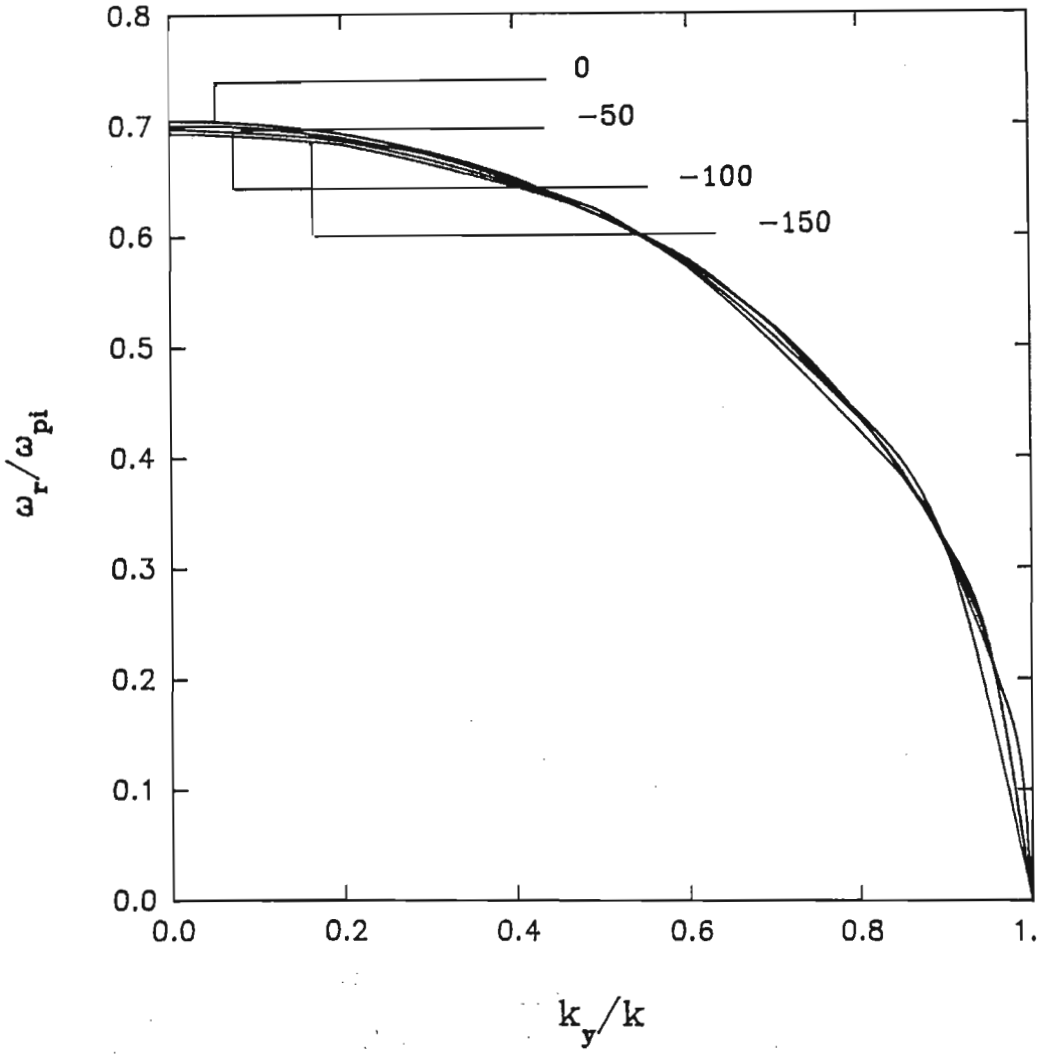

Figure 5.1: Normalized real frequency as a function of k_y/k for the IAI with $v_{dbz} = 100C_s$ and $v_{dhz} = 0, -50, -100$ and -150. Other fixed parameters are as for figure (4.1).

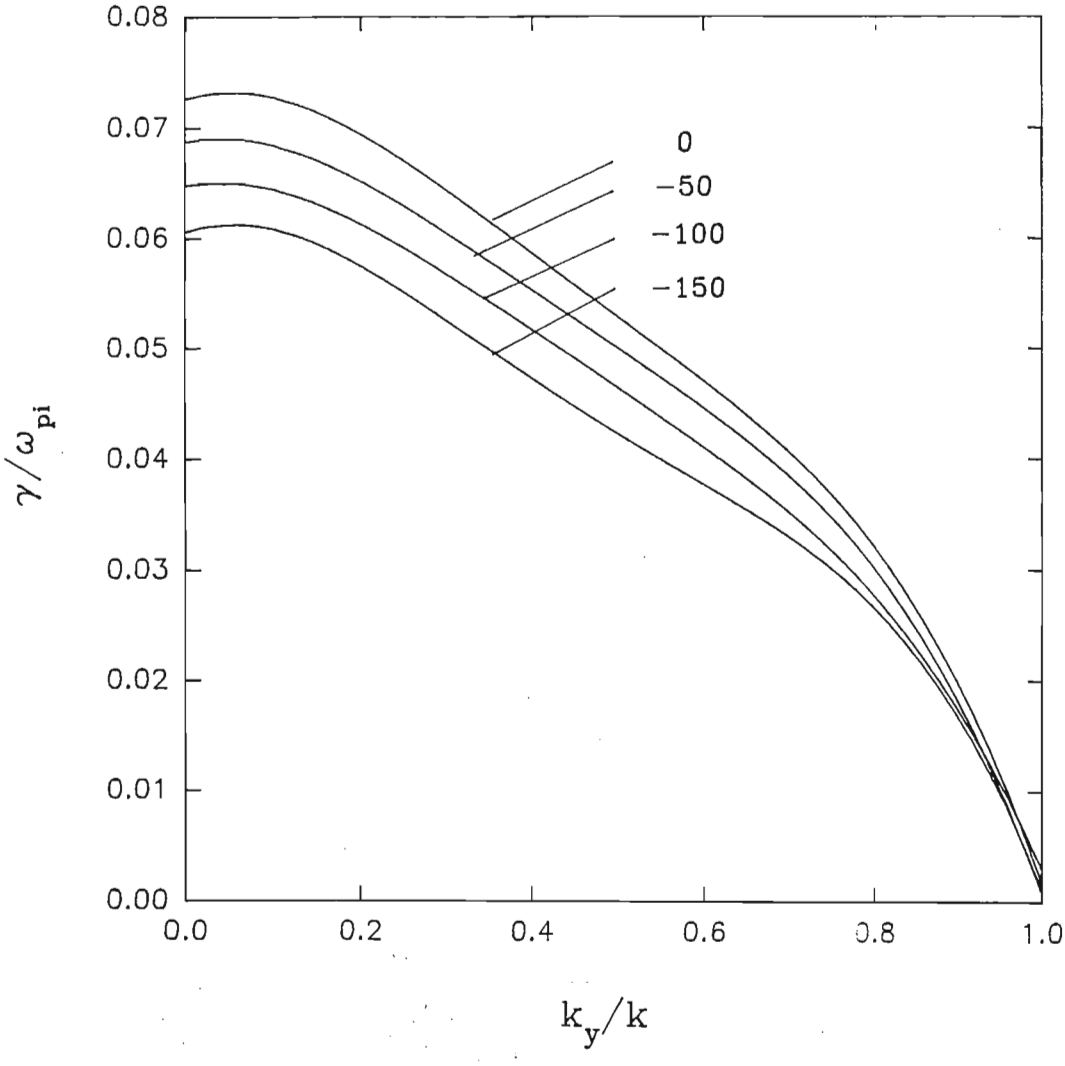

Figure 5.2: Normalized growth rate as a function of k_y/k for the IAI with $v_{dbz} = 100C_s$. The parameter labelling the curves is v_{dhz}. Other fixed parameters are as for figure (4.1).

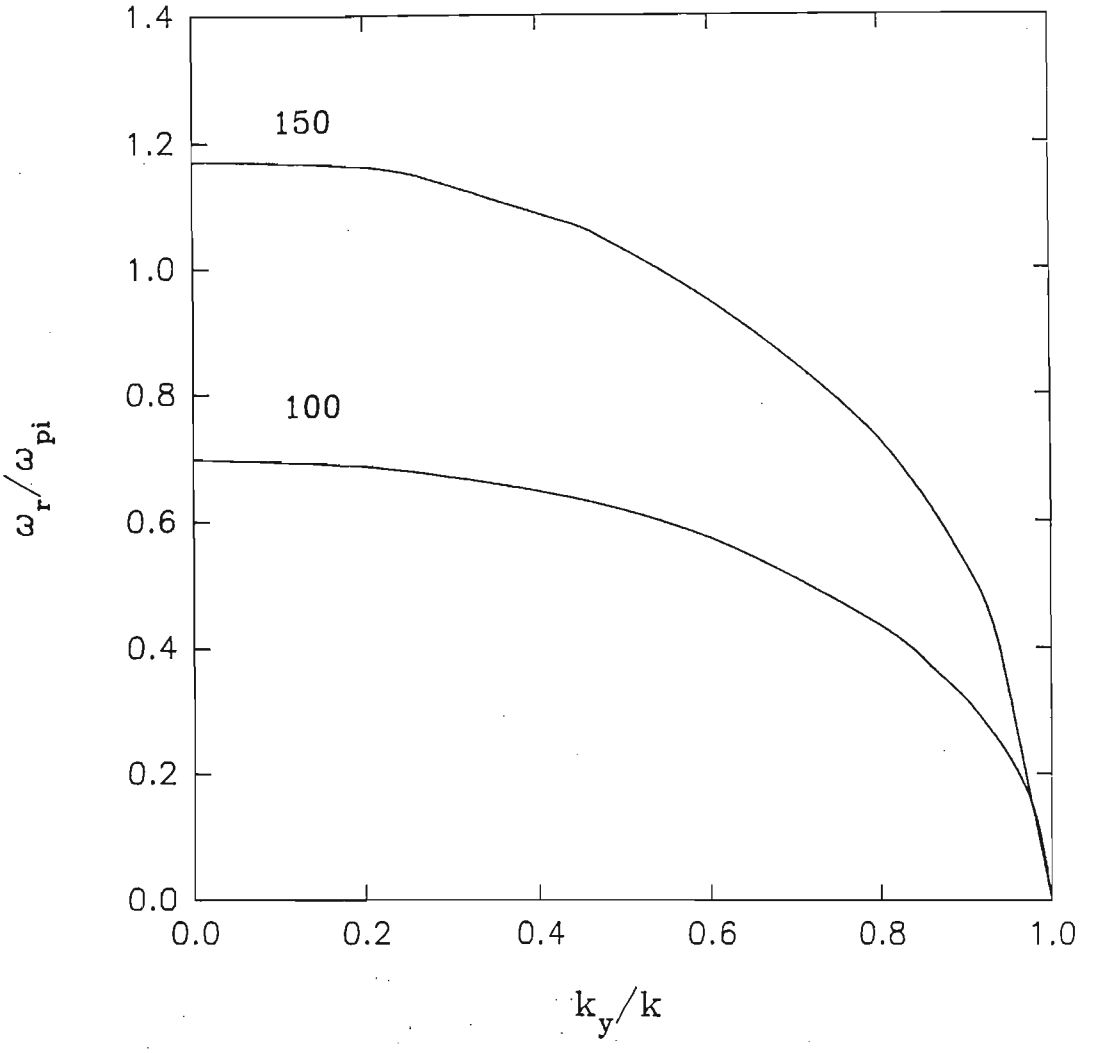

Figure 5.3: Normalized real frequency as a function of k_y/k for the IAI with $v_{dhz} = -100C_s$. The parameter labelling the curves is v_{dbz}. Other fixed parameters are as for figure (4.1).

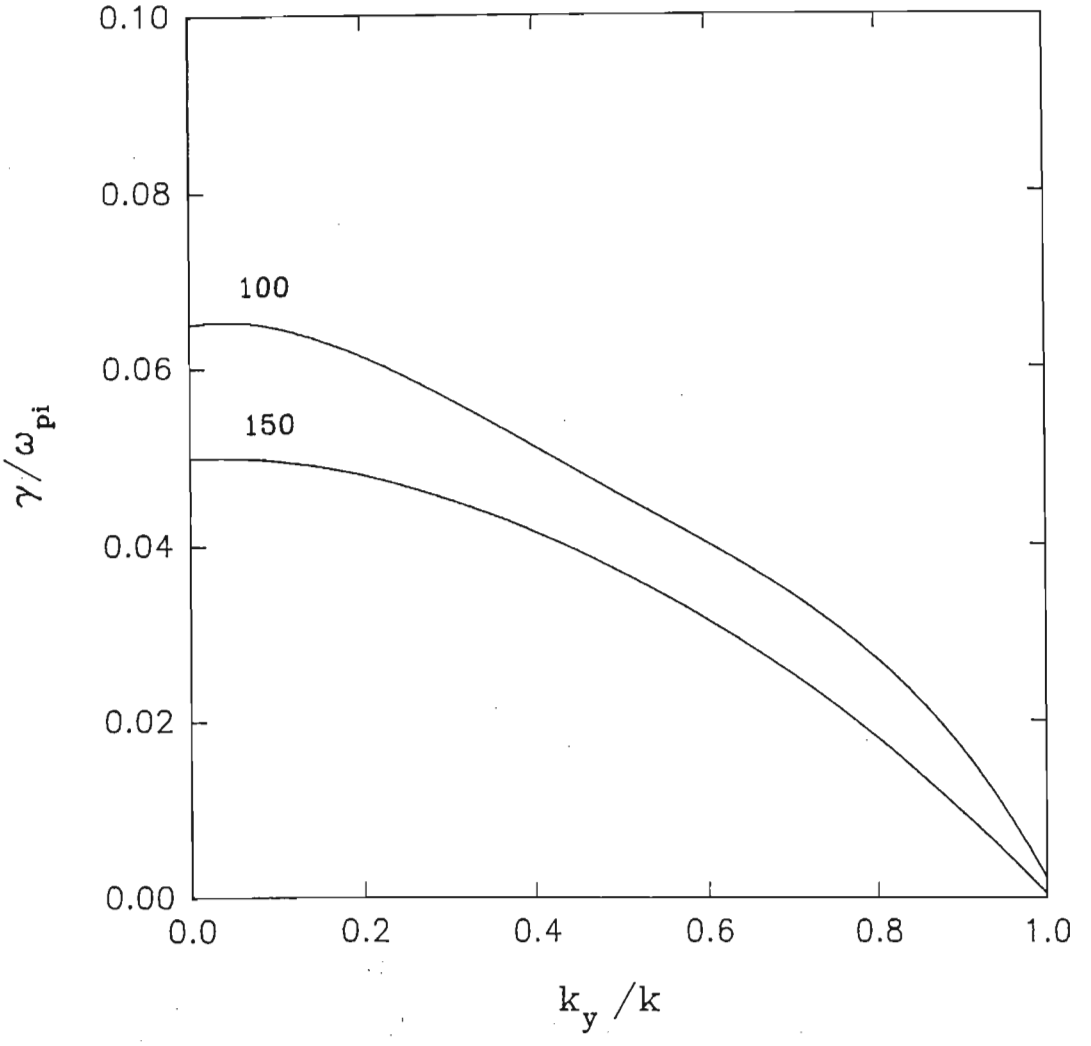

Figure 5.4: Normalized growth rate as a function of k_y/k for the IAI with $v_{dhz} = -100C_s$. The parameter labelling the curves is v_{dbz}. Other fixed parameters are as for figure (4.1).

drift velocity, γ/ω_{pi} attains a maximum of 0.1435 at $n_{co} = 0.006$ for parallel propagation, while for stationary hot electrons $(\gamma/\omega_{pi})_{max}$ is 0.142 also at $n_{co} = 0.006$. For almost perpendicular propagation the results were found to be similar. These curves show that the density of the background electrons at which the instability obtains its maximum growth rate is negligibly affected by the drift velocity of the hot electrons.

5.2.3 The effect of the hot electron temperature, T_h/T_c

Figure (5.7) shows the normalized growth rate versus normalized k for hot electron temperatures of $T_h/T_c = 1000$, 500, 100 and 50 at $k_y/k = 0.0$. Here also, the ion beam drift velocity was set at $100C_s$ and the electron drift velocity set at -$100C_s$. The shape of the curves are similar to those of figure (4.12) in chapter 4. However, we note that there is a general increase in the maximum growth rate attained for the various hot electron temperatures. The increase in the growth rate may be associated with the decrease in electron Landau damping. The slow ion acoustic wave 'sees' the negative slope of the hot electron velocity distribution function, $f_{eh}(v_z)$ 'flatten' as $T_h(C_h = \sqrt{\frac{T_h}{me}})$ increases and therefore $(\partial f_{eh}/\partial v_z)$ decreases. This reduces electron damping, hence enhancing the growth rate.

5.2.4 The effect of the ion beam temperature

With $k_y/k = 0.0$, the hot electron temperature, $T_h/T_c = 1000$, $v_{dbz} = 100C_s$ and $v_{dhz} = -100C_s$ we examined the effect of increasing the ion beam temperature on the instability. Again, as in chapter 4, for increasing ion beam temperature, we note the drop in the maximum growth rate for the curves shown in figure (5.8). This is consistent with the condition $T_e/T_b >> 1$ for the ion acoustic instability. A general increase in the maximum for each choice of temperature seen here as compared to

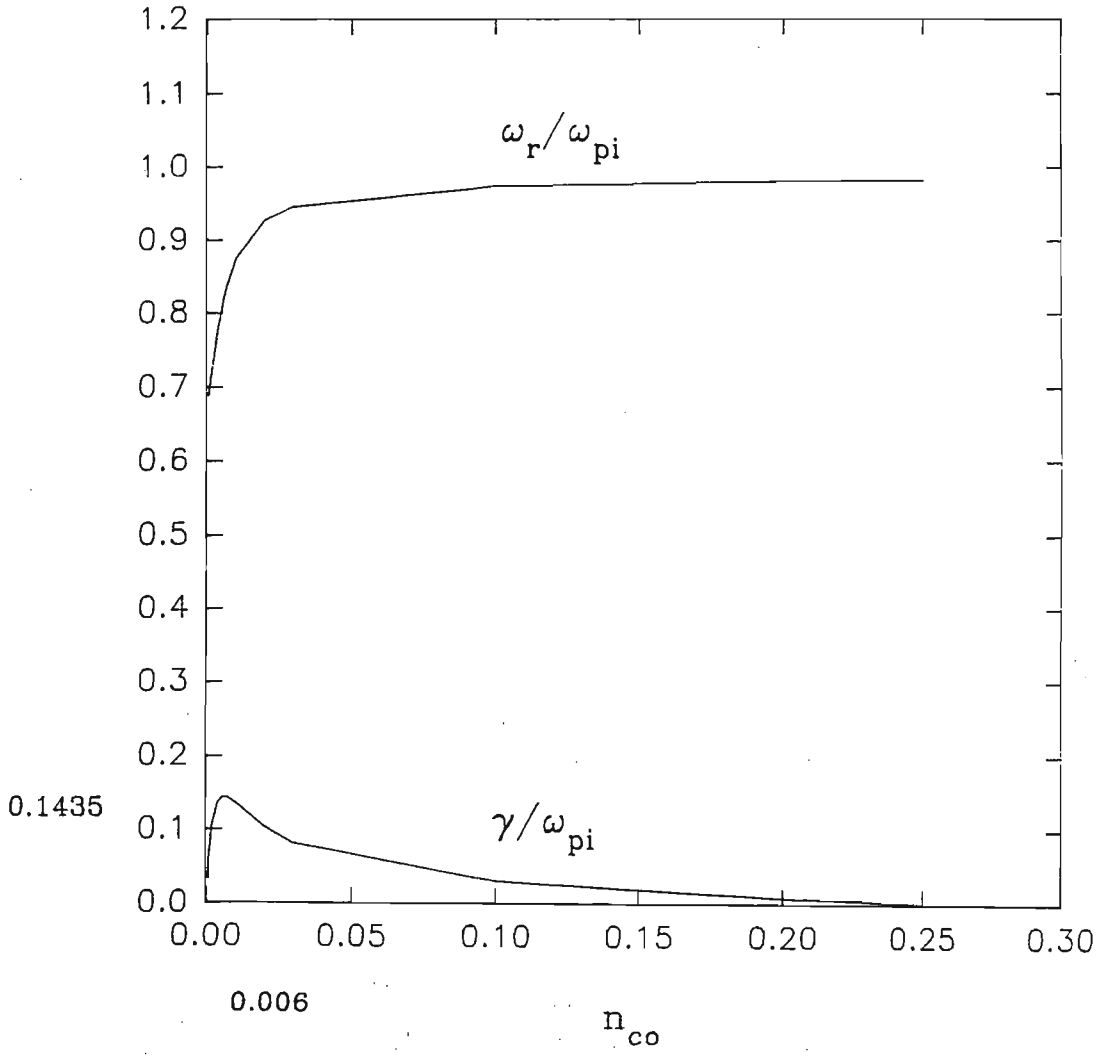

Figure 5.5: Normalized real frequency and growth rate as a function of cold electron density, n_{co}, for the IAI at $k_y/k = 0.0$, $v_{dbz} = 100C_s$ and $v_{dhz} = -100C_s$. The maximum growth rate is 0.1435 at a density of 0.006. Other fixed parameters are as for figure (4.1).

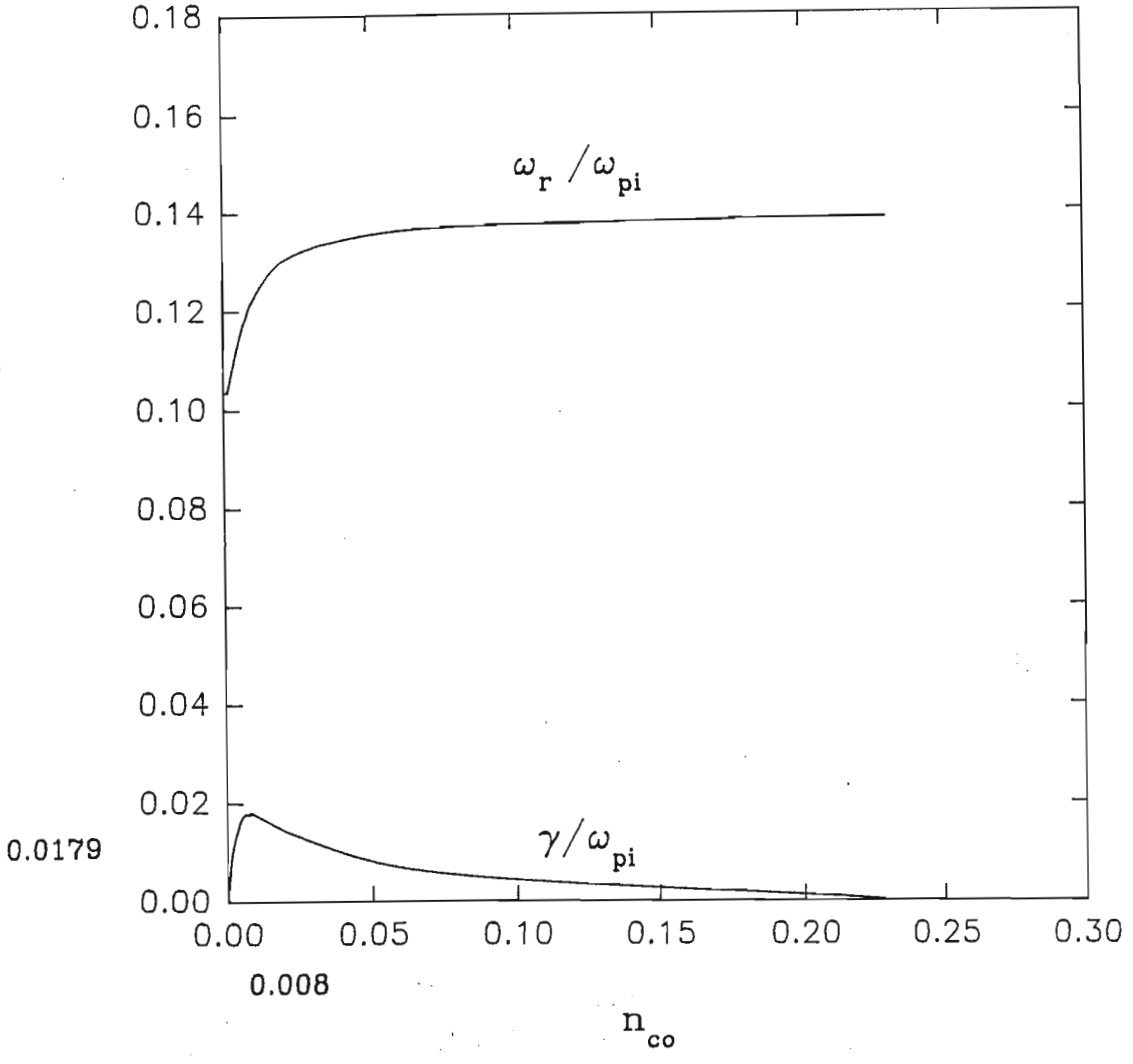

Figure 5.6: Normalized real frequency and growth rate as a function of cold electron density, n_{co}, for the IAI at $k_y/k = 0.99$, $v_{dbz} = 100C_s$ and $v_{dhz} = -100C_s$. The maximum growth rate is 0.01798 at a density of 0.008. Other fixed parameters are as for figure (4.1).

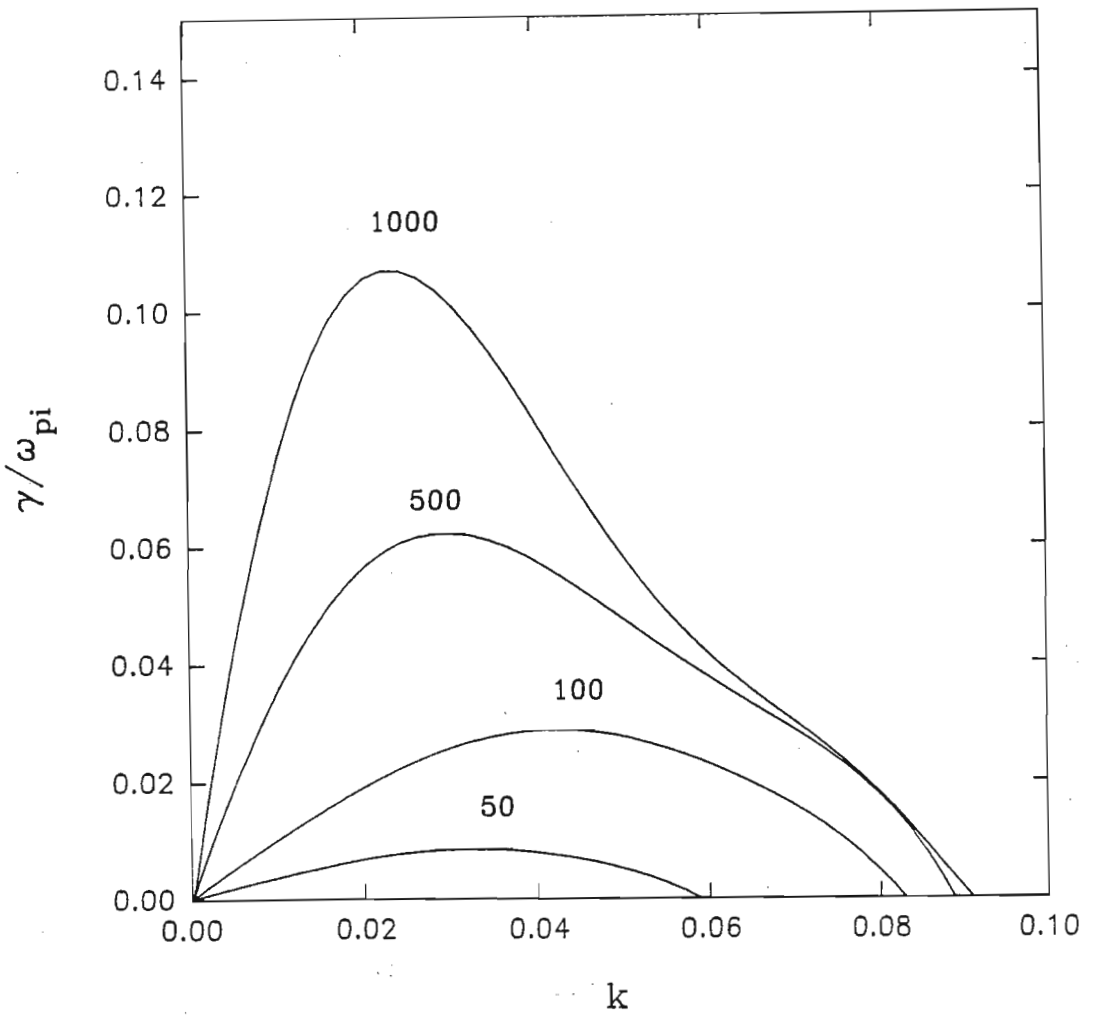

Figure 5.7: Normalized growth rate as a function of k for the IAI at $k_y/k = 0.0, v_{dbz} = 100C_s$ and $v_{dhz} = -100C_s$. The parameter labelling the curves is T_h/T_c. Other fixed parameters are as for figure (4.1).

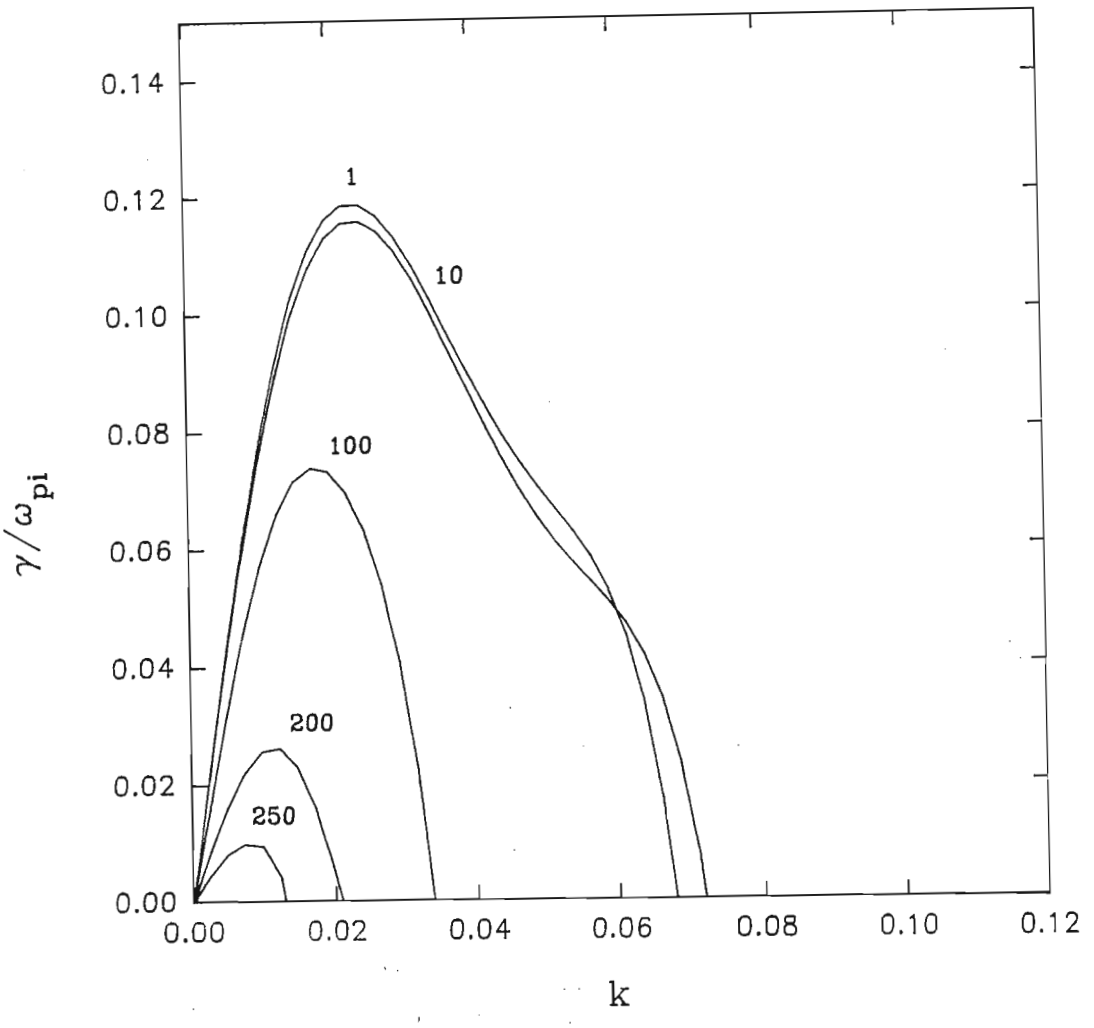

Figure 5.8: Normalized growth rate as a function of k for the IAI. The parameter labelling the curves is T_b/T_c. Other fixed parameters are as for figure (5.7).

the curves in figure (4.16) of chapter 4 is observed. We again attribute this to the decrease in electron Landau damping as v_{dhz} is increased.

5.3 The modified two-stream instability (MTSI)

5.3.1 Variation of propagation angle, $_y$

With the electron drift velocity $v_{dhz} = -150C_s$, the curves were plotted for the ion beam drift velocity set at $150C_s$ and $180C_s$. We note from our studies in chapter 4 that the MTSI is excited for ion beam drift speeds in the chosen range. From figures (5.9) and (5.10), we see that the MTSI is sensitive to the changes in the ion beam drift velocity, v_{dbz}.

As in chapter 4, we find that as v_{dbz} is increased, the real frequency and growth rate increases. This is consistent with the behaviour of the MTSI which has the phase velocity close to that of the slow ion beam instability (Bergmann et.al (1988)). The fact that the growth rate attains a maximum for a k_y/k value very much oblique to $\mathbf{B_o}$ and not at $k_y/k = 0$ as for the IAI, confirms that the instability is the MTSI.

From figure (5.11) we find that unlike the case of the IAI, for the MTSI, increasing the magnitude of the negative electron drift velocity, v_{dhz}, increases rather than decreases the growth rate. This is a characteristic of the MTSI which is a non-resonant instability driven simply by the relative streaming of the particles. As the counter-streaming electron velocity increases, this increases the relative velocity between the ions and the electrons, hence enhancing the growth rate.

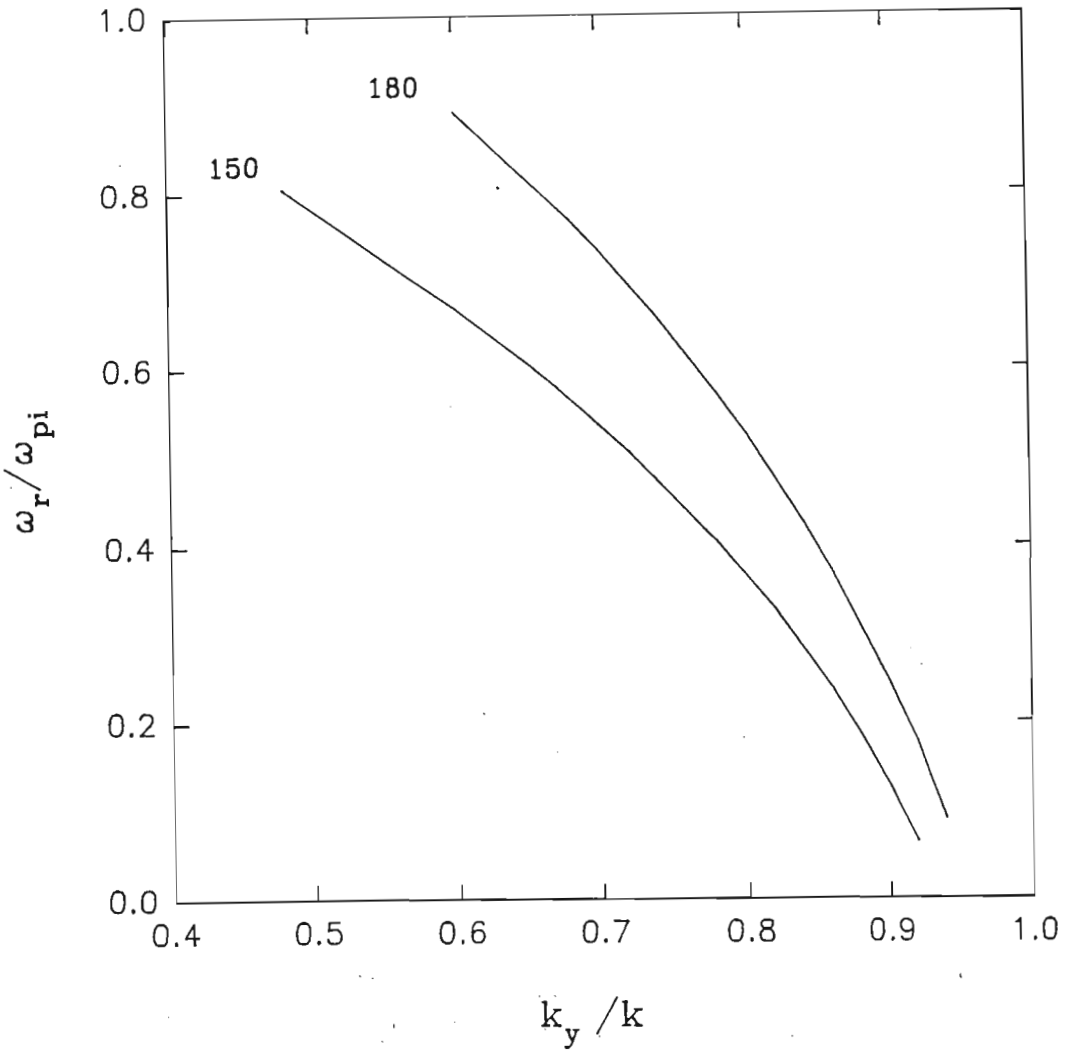

Figure 5.9: Normalized real frequency as a function of k_y/k for the MTSI with $v_{dhz} = -100C_s$. The parameter labelling the curves is v_{dbz}. Other fixed parameters are as for figure (4.1).

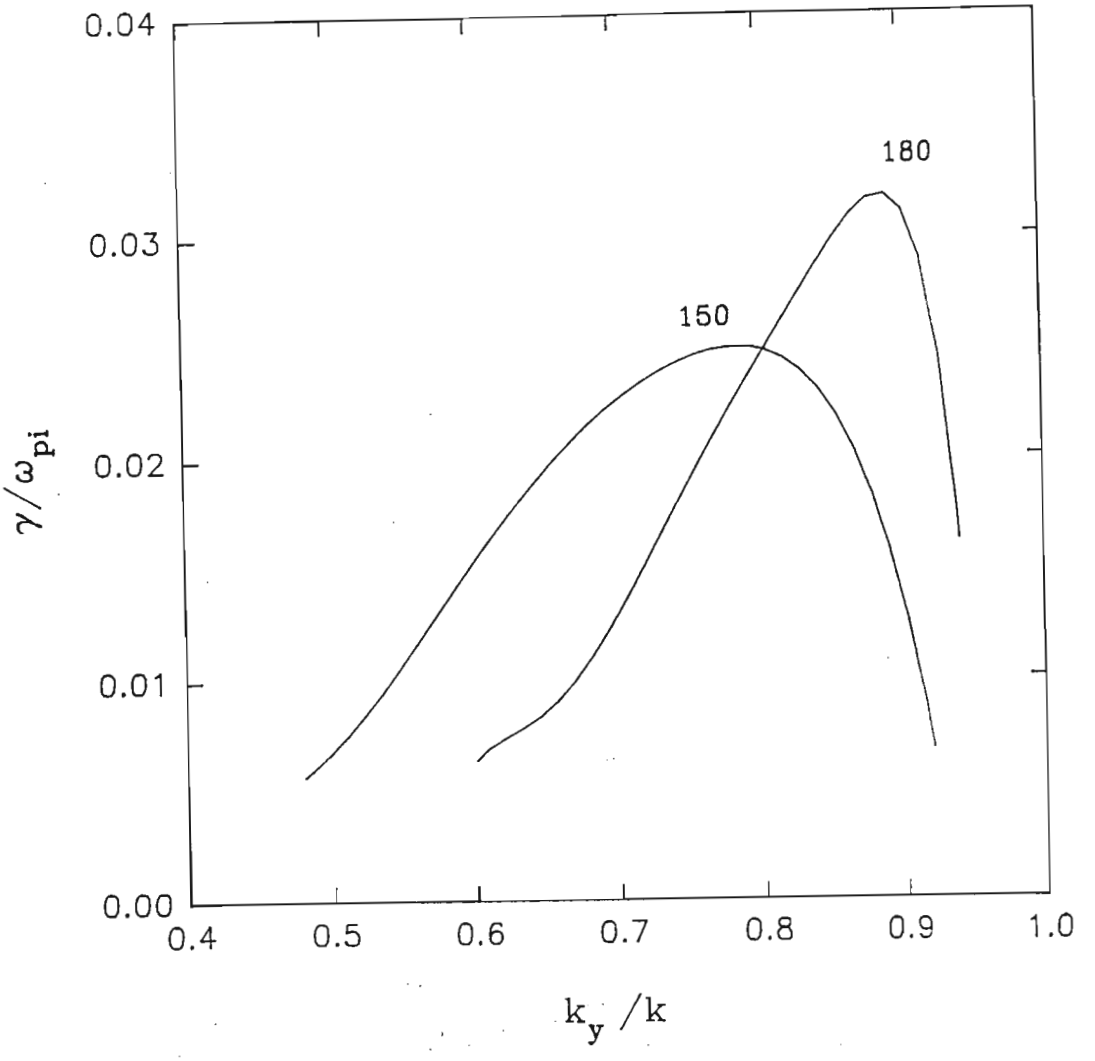

Figure 5.10: Normalized growth rate as a function of k_y/k for the MTSI with $v_{dhz} = -100C_s$. The parameter labelling the curves is v_{dbz}. Other fixed parameters are as for figure (4.1).

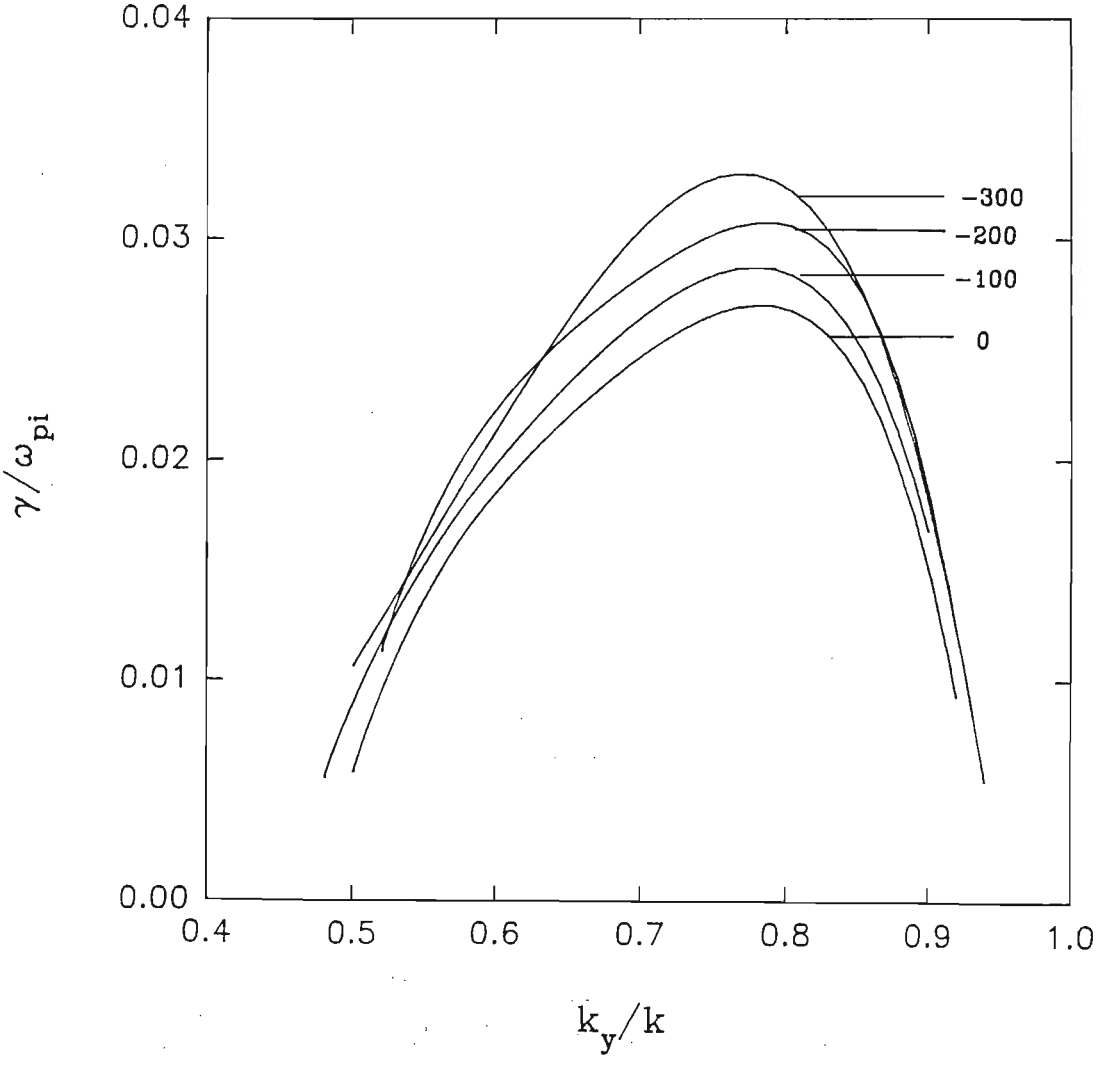

Figure 5.11: Normalized growth rate as a function of k_y/k for the MTSI with $v_{dbz} = 200C_s$. The parameter labelling the curves is v_{dhz}. Other fixed parameters are as for figure (4.1).

5.3.2 The effect of varying the cold background electron density, n_{co}

In this study, the electron drift velocity was set at -$100C_s$, the ion beam drift velocity set at $200C_s$ and $k_y/k = 0.9$. Here we find that the curves in figure (5.12) are similar to those in figure (4.21) of chapter 4. At a density of 0.0036, the growth attains a maximum of 0.0543.

5.3.3 The effect of the hot electron temperature, T_h/T_c

When comparing the results of this study (figure (5.13)) with those in chapter 4 (figure (4.22)), we find that there is a drop in the maximum growth rate for $T_h/T_c =$ 1000 and $(\gamma/\omega_{pi})_{max}$ shifts to lower k values. Also, we find that the lower threshold temperature for the instability to propagate is higher in the presence of the counter-streaming hot electrons.

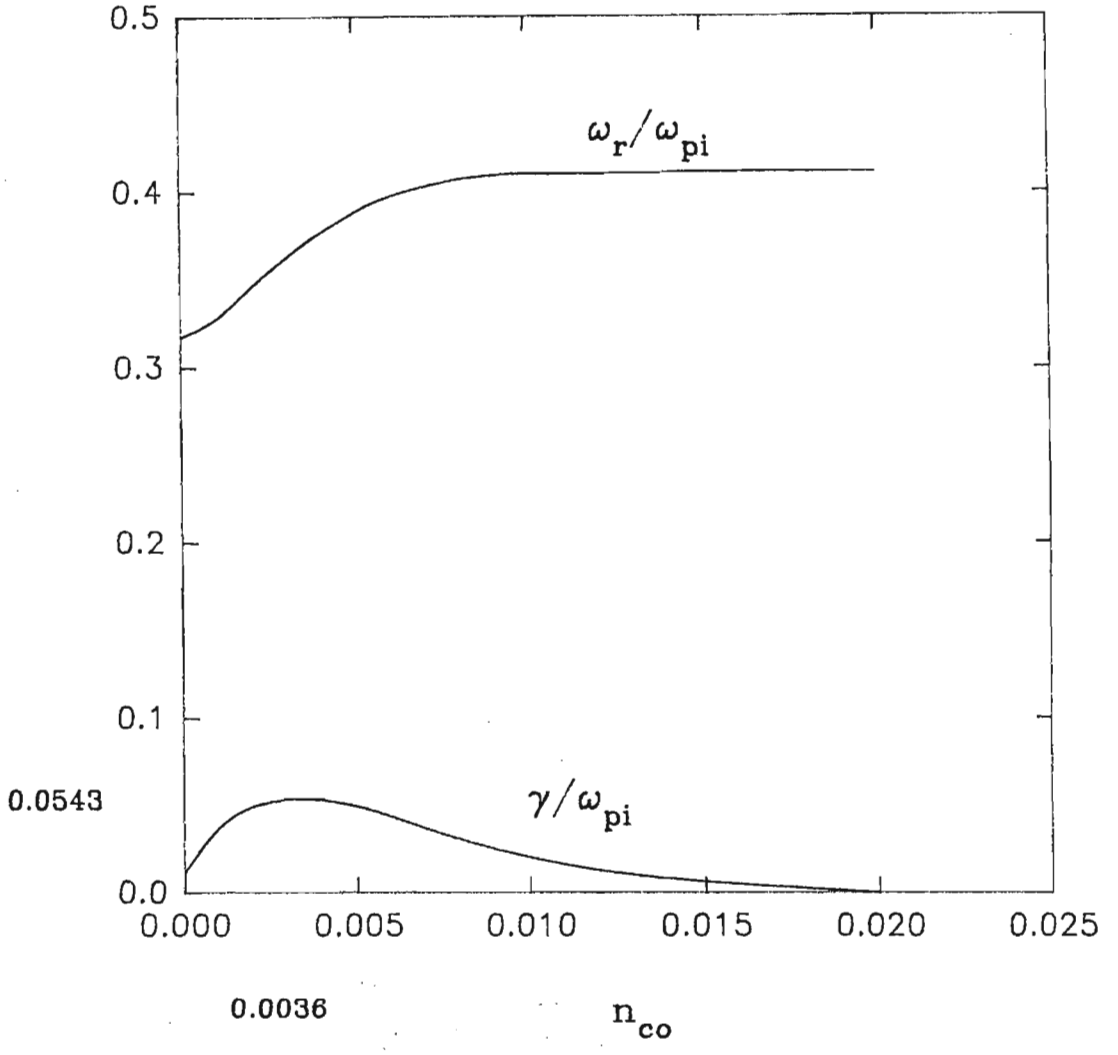

Figure 5.12: Normalized real frequency and growth rate as a function of cold electron density, n_{co}, for the MTSI at $k_y/k = 0.9$, $v_{dbz} = 200C_s$ and $v_{dhz} = -100C_s$. Other fixed parameters are as for figure (4.1).

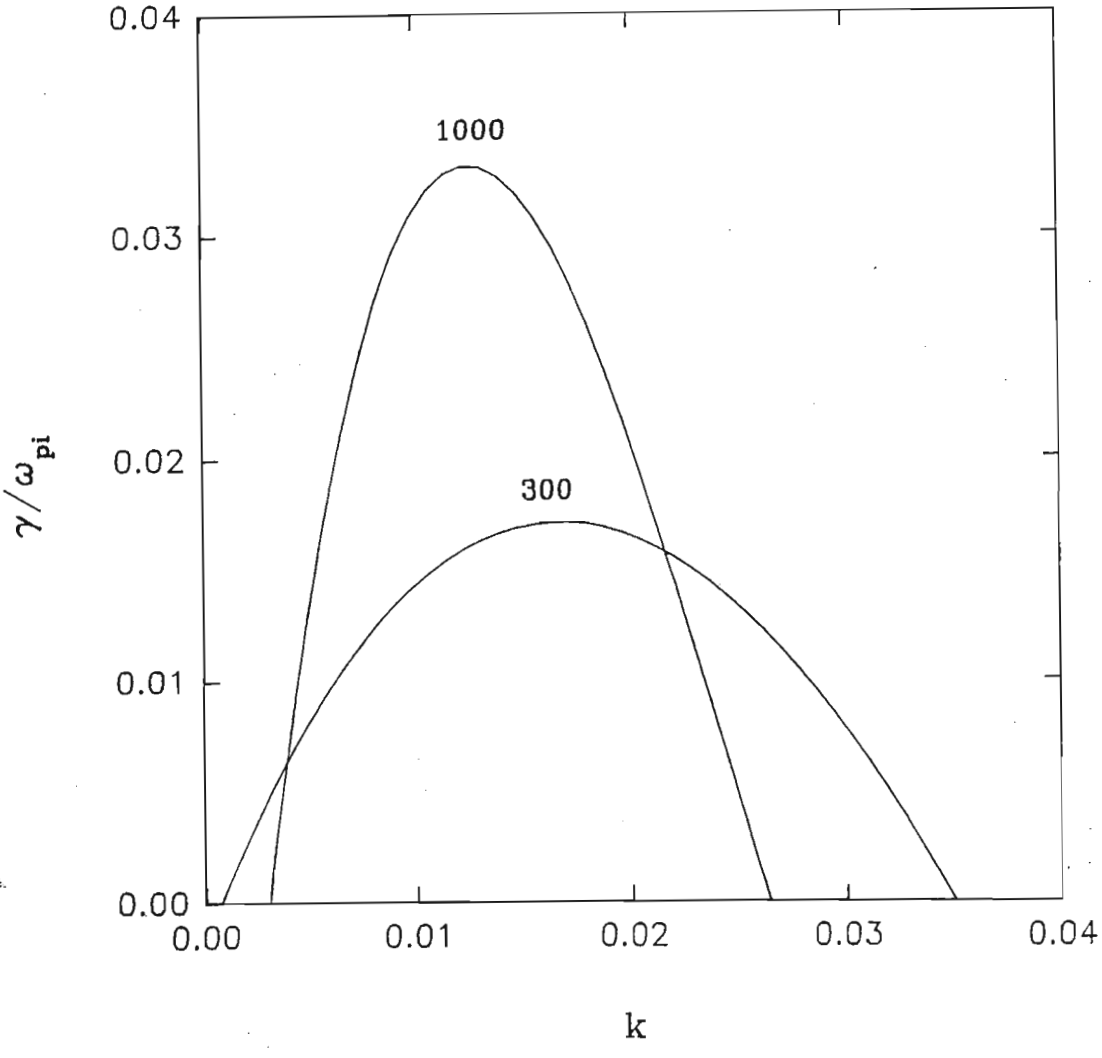

Figure 5.13: Normalized growth rate as a function of k for the MTSI at $k_y/k = 0.9, v_{dbz} = 200C_s$ and $v_{dhz} = -100C_s$. The parameter labelling the curves is T_h/T_c. Other fixed parameters are as for figure (4.1).

Chapter 6

Conclusion

In this thesis we have examined low frequency electrostatic instabilities present in a three species plasma consisting of precipitating hot electrons, cold stationary electrons and a cool ion beam that is modelled on observations of the auroral plasma. The kinetic dispersion relation was derived and numerically solved without approximations. The instability was initially driven by an ion beam drift along the external magnetic field, $\mathbf{B_o}$.

Two instabilities were found to be present, viz. a resonant slow beam ion acoustic instability and a non-resonant modified two stream instability. The behaviour of these instabilities were investigated in chapter 4 and chapter 5 through a parameter variation study.

In chapter 4, the study was carried out with stationary hot electrons and cool drifting ions. The slow IAI featured prominantly at the normalized drift velocity of about $23C_s$ to $230C_s$ for a large spread of the angle of propagation relative to $\mathbf{B_o}$, k_y/k. Beyond $230C_s$, a simple beam instability propagated at the phase velocity for a broad range of the ion beam drift velocity. A study of the effect of varying the propagation

vector revealed that for angles of propagation oblique to the ion beam drift velocity, the maximum growth rate, γ/ω_{pi}, decreases significantly. This was expected since for the IAI maximum resonance is in the direction parallel to the drift velocity.

We next examined the effect of varying the cold electron density, n_{co}, on the IAI. Optimum values of n_{co} for maximum growth rate were found for both parallel and near perpendicular propagation. It was also found that the plasma was unstable in in the absence of the cold electron component (i.e. $n_{co} = 0$).

The instability growth rate was found to be proportional to the hot electron temperature (associated with hot electron inverse Landau damping), but inversely proportional to the ion beam temperature (associated with ion Landau damping). These results were significant since in the auroral plasma, the temperature of the plasma species varies at different altitudes (Bergmann and Lotko,1986).

A similar parameter variation study was made of the second plasma instability that was found to dominate at drift velocities higher than about $140C_s$ and for large propagation angles relative to $\mathbf{B_o}$. The results were consistent with the characteristics of the modified two-stream instability, (MTSI). The instability was observed to propagate in a narrow cone about the perpendicular to $\mathbf{B_o}$ with a strong θ- dependence.

Here as well, an optimum value of n_{co} was found for which the growth rate attained a maximum. The study of the effect of increasing the hot electron temperature showed that the mode grows with increasing hot electron temperature.

In chapter 5 we examined the effect of counter-streaming hot electrons on the instabilities studied in chapter 4. It was found for the IAI that increasing the electron drift

velocity caused a decrease in the growth rate but a neglible change in the real frequency curves. This is an expected result, since from the theory, the real frequency of the slow beam IAI depends only on the ion beam drift velocity and not on the electron drift velocity. Changes in the growth rate has been attributed to increased electron Landau damping. The results with regards to variation of the cold electron density and hot electron temperature were similar to those of chapter 4.

On the other hand, for the MTSI, we find that the growth rate is enhanced as we increase both the ion drift velocity as well as the electron drift velocity. This is not surprising since the (non-resonant) instability is driven by the relative streaming of particles. Therefore we find that as the magnitudes of the relative drifts are increased, the growth rate also increases.

The curves depicting the variation of the cold electron density were also similar to those of chapter 4. It was significant to note that for the MTSI, the decrease of the hot electron temperature, T_h/T_c, caused a diminishing of the maximum growth rate for a chosen temperature. Also, at the chosen propagation vector value, k = 0.9, the minimum value of T_h for positive growth was higher in the presence of counter-streaming electrons.

The results of our study is an extension of the work of Lakhina, (1993). In his paper, Lakhina discusses (1) fluid instabilities driven by an ion beam and (2) a resonant instability driven by hot electrons. In our investigation, we found the presence of two low- frequency plasma instabilities, viz. the slow ion acoustic instability and the modified two-stream instability. The instabilities are kinetic and driven by the cool ion beam. Their presence may be associated with the low-frequency electric field fluctuations (LEFs)that have been observed in the auroral plasma.

The model that we have adopted may be extended to include a counter-streaming O^+ ion beam. Ion-ion waves in the auroral region have been investigated by Dusenbury et.al.(1988), Ashour-Abdalla et.al.(1989) and Hultqvist et.al.(1991) among others. Further, the non-linear evolution of these instabilities, leading to the possible formation of, for example, solitons and doubles layers is worthy of investigation.

References

[1] Ashour-Abdalla,M. and D.Schriver, *Geophys.Res.Lett.*, **19** , 21-24, 1989.

[2] Bergmann.R., and W.Lotko, *J.Geophys.Res.*, **91** , 7033, 1986.

[3] Bergmann,R., I.Roth and M.K.Hudson, *J.Geophys.Res*, **93** , 4005-4020, 1988.

[4] Bhatia,K.G. and G.S.Lakhina, *J.Plasma Phys.*, **24**, 221, 1980.

[5] Dusenbery,P.B., R.E.Martin Jr. and R.M.Winglee, *J.Geophys.Res.* , **93**, 5655, 1988 .

[6] Fried,B.D. and S.D.Conte, *The Plasma Dispersion Function*, Academic Press, New york, 1961.

[7] Gary,S.P. and N.Omidi, *J. Plasma Phys.*, **37**, 45, 1987.

[8] Gary,S.P. and J.J.Sanderson, *J.Plasma Phys.*, **4**, 739, 1970.

[9] Hultqvist,B., *J.Geophys.Res.*, **93**, 9777-9784, 1988.

[10] Hultqvist,B., R.Lundin, K.Stasiewics, L.Block, P.A.Lindqvist, G.Gustafsson, H.Koskinen, A.Bahnsen, T.A. Potemra and L.J.Zanetti, *J.Geophys.Res.* , **93**, 9765-9776, 1988.

[11] Iranpour,K., H.L.Pecseli, J.Trulsen, A.Bahnsen, F.Primdahl and K.Rinnert, *Ann.Geophys.*, **15** , 878-889, 1997.

[12] Lakhina,G.S.,*Physica Scripta.*, **T50**,114-126,1994.

[13] Lakhina,G.S., *Ann.Geophys.*, **11**, 705, 1993.

[14] McBride,J.B., E.Ott, J.P. Boris and J.H.Orens, *Phys. Fluids*, **15**, 2367, 1972.

[15] Mozer,F.S., C.W.Carlson, M.K.Hudson, R.B.Torbert, B.Parady and J.Yatteau, *Phys.Rev.Lett.*, **38**, 292, 1977.

[16] Rose,G., K.Schlegel, K.Rinnert, H.Kohl, E.Nielsen, G.Dehmel, A.Friker, F.J.Lübken, H.Lühr, E.Neste and A.Steinweg, *J.Atmos.Terr.Phys.* , **54**, 657, 1992.

[17] Singh,P. and R.Bharuthram, *J.Plasma Phys.*, **44**, 77-90, 1990.

[18] Singh,P, R.Bharuthram and M.A.Hellberg, *J.Plasma Phys.* **44**, 61-75, 1990.

[19] Temerin,M.,*J.Geophys.Res.*, **83**,2609,1978

[20] Watson,G. *A Treatise on the Theory of Bessel Functions* , Cambridge University Press, 2nd Edition, 1944.